

# Theoretical Analysis of Measure Consistency Regularization for Partially Observed Data

Yinsong Wang, and Shahin Shahrampour, *Senior Member, IEEE*

**Abstract**—The problem of corrupted data, missing features, or missing modalities continues to plague the modern machine learning landscape. To address this issue, a class of regularization methods that enforce consistency between imputed and fully observed data has emerged as a promising approach for improving model generalization, particularly in partially observed settings. We refer to this class of methods as Measure Consistency Regularization (MCR). Despite its empirical success in various applications, such as image inpainting, data imputation and semi-supervised learning, a fundamental understanding of the theoretical underpinnings of MCR remains limited. This paper bridges this gap by offering theoretical insights into why, when, and how MCR enhances imputation quality under partial observability, viewed through the lens of neural network distance.

Our theoretical analysis identifies the term responsible for MCR’s generalization advantage and extends to the imperfect training regime, demonstrating that this advantage is not always guaranteed. Guided by these insights, we propose a novel training protocol that monitors the duality gap to determine an early stopping point that preserves the generalization benefit. We then provide detailed empirical evidence to support our theoretical claims and to show the effectiveness and accuracy of our proposed stopping condition. We further provide a set of real-world data simulations to show the versatility of MCR under different model architectures designed for different data sources.

**Index Terms**—Imputation, Integral Probability Metric, Neural Net Distance, Measure Consistency Regularization

## I. INTRODUCTION

Rapid advances in data acquisition technologies ranging from high-resolution cameras and environmental sensors to transmission electron microscopy and single-cell sequencing have fueled an unprecedented boom in data generation, forming the backbone of modern machine learning and artificial intelligence. Yet, despite this explosion in data volume, a persistent and troubling issue remains: missing data, where features are unobserved or lost. This problem is pervasive across domains and has only become more pronounced as data grows richer and more multimodal. In single-cell biology, for example, the historical norm was to profile each cell with only one omic technology, such as gene expression, chromatin accessibility, or protein abundance, leading to missing modalities, which are effectively missing features. Truly multimodal single-cell datasets have only begun to emerge in recent years [1], [2], highlighting how deeply entrenched this limitation has been. Moreover, the issue is not confined to specialized fields:

Y. Wang is with the H. Milton Stewart School of Industrial & Systems Engineering at Georgia Institute of Technology, Atlanta, GA 30332 USA.  
E-mail: ywang4542@gatech.edu

S. Shahrampour is with the Department of Mechanical and Industrial Engineering at Northeastern University, Boston, MA 02115 USA.  
E-mail: s.shahrampour@northeastern.edu

more than 40% of datasets in the UCI Machine Learning Repository contain missing values [3], emphasizing the ubiquity of missingness even in widely used benchmark datasets.

The most direct approach to handling missing data is imputation. Formally, the problem can be described using two datasets: (i) a fully observed dataset,  $\mathbf{D}_l = \{(\mathbf{x}_i, \mathbf{z}_i)\}_{i=1}^n$ , consisting of  $n$  data points where  $\mathbf{x} \in \mathcal{X} \subseteq \mathbb{R}^{d_x}$  and  $\mathbf{z} \in \mathcal{Z} \subseteq \mathbb{R}^{d_z}$  are two sets of features; and (ii) a partially observed dataset,  $\mathbf{D}_u = \{\mathbf{x}_i\}_{i=n+1}^{n+m}$ , of  $m$  data points for which  $\mathbf{z}$  is missing. The imputation goal is to construct a prediction function  $f$  that can recover or approximate the unobserved features. A wide range of methods have historically been proposed for this task, often tailored to specific missing-data patterns. Classical examples include K-nearest neighbors (KNN) imputation [4], regression-based approaches [5], and multiple regression techniques [6], among others.

The recent explosion in both data volume and dimensionality has motivated various research communities to develop domain-specific solutions to the missing data imputation problem. Examples span computer vision [7]–[10], sensor networks [11], [12], and single-cell data integration [13]–[15]. Although these efforts share a common underlying mathematical formulation, the problem often appears under different names, such as image inpainting [16], cross-modal imputation [17], imputation with structured missingness [18], RNA imputation [19], or missing channel reconstruction [20]. A unifying characteristic across much of this literature, however, is that the partially observed dataset  $\mathbf{D}_u$  is typically leveraged only as an auxiliary resource for model testing or supporting downstream learning tasks after imputation, rather than being directly employed to improve the imputation quality itself.

Interestingly, a bespoke practice explicitly leverages the partially observed dataset  $\mathbf{D}_u$  to enhance imputation quality. This simple, practical approach lacks a formal name or a theoretical foundation despite its prevalence across domains. The central idea is intuitive: to improve imputation, one can impose a regularization constraint requiring that the empirical measure of the imputed dataset derived from  $\mathbf{D}_u$  remains consistent with that of the fully observed dataset  $\mathbf{D}_l$ . In this work, we refer to this strategy as *measure consistency regularization (MCR)*, which we will formally introduce in Section II. Although this idea has achieved notable empirical success in many applications [21]–[24], its theoretical properties has remained elusive, leaving open fundamental questions about why, when, and how it works.

To address this theoretical gap, we undertake a comprehensive analysis of MCR through the lens of the *neural net distance (NND)* [25], due to its generality and theoretical properties.

NND represents a broad class of discrepancy measures that can serve as effective consistency regularizers. Building on this foundation, we summarize our main contributions as follows:

- We provide a unified view on imposing MCR between imputed data and observed data by incorporating NND as a penalty function in the learning objective. This formulation generalizes several existing approaches [22], [26] that demonstrated strong empirical effectiveness.
- We establish the *first known* estimation error bound for MCR training in Theorem 1 under mild assumptions. This bound highlights the model-agnostic and distribution-agnostic robustness of learning predictive functions from partially observed data. Specifically, it shows that an estimation error term decays at a rate of  $1/\sqrt{m+n}$ , where  $n$  denotes the number of fully observed data points, and  $m$  denotes the number of partially observed data points.
- We extend this estimation error analysis to the imperfect training scenario in Theorem 2, where the training loss converges to a small but non-zero value. Our results reveal that the robustness advantage of imperfect MCR training is not always guaranteed. However, building on this insight, we propose a formal MCR training protocol that leverages the *duality gap* to ensure consistent robustness benefits.
- We conduct extensive simulations to evaluate multiple aspects of our theoretical analysis and the proposed training protocol. In addition, we demonstrate the versatility of MCR on several real-world datasets.

### Preliminaries and Notations

We denote the true joint probability measure of the fully observed dataset by  $\pi(\mathbf{x}, \mathbf{z})$ , or simply  $\pi$ . The joint measure induced by a prediction function  $f$  is denoted as  $\pi(\mathbf{x}, f(\mathbf{x}))$ , abbreviated as  $\pi^f$  to emphasize the dependence on  $f$ . The empirical joint measure of the fully observed dataset is denoted by  $\pi_l$ , while the empirical joint measure of the partially observed data (imputed by  $f$ ) is denoted by  $\pi_u^f$ . We further denote the empirical distribution of the mixture dataset by  $\pi_{ul}^f$ . Specifically, we have

$$\begin{aligned}\pi_l &:= \frac{1}{n} \sum_{i=1}^n \delta_{(\mathbf{x}_i, \mathbf{z}_i)} \\ \pi_u^f &:= \frac{1}{m} \sum_{i=n+1}^{n+m} \delta_{(\mathbf{x}_i, f(\mathbf{x}_i))} \\ \pi_{ul}^f &:= \frac{1}{n+m} \sum_{i=1}^{n+m} \delta_{(\mathbf{x}_i, f(\mathbf{x}_i))}.\end{aligned}$$

For any probability measure  $\pi$  on  $(\mathcal{X}, \mathcal{Z})$  and any integrable function  $f$ , we write  $\pi f := \mathbb{E}_\pi[f]$ , where  $\mathbb{E}[\cdot]$  denotes the expectation operator.

## II. MEASURE CONSISTENCY REGULARIZATION WITH NEURAL NET DISTANCE

### A. Imputation without Regularization

The learning objective of interest is essentially a supervised learning task to learn a prediction function  $f^* : \mathcal{X} \rightarrow \mathcal{Z}$  such

that

$$f^* = \operatorname{arginf}_{f \in \mathcal{F}} \{\pi \mathcal{L}^f\},$$

where  $\mathcal{L}^f$  denotes the loss  $\mathcal{L}$  evaluated on the predictions of  $f$ . Because the true distribution  $\pi$  is unavailable in practice, the common approach is empirical risk minimization (ERM), which yields the proxy solution

$$f_l^* = \operatorname{arginf}_{f \in \mathcal{F}} \{\pi_l \mathcal{L}^f\}, \quad (1)$$

based on the empirical distribution  $\pi_l$  of fully observed data.

The distinction between imputation and standard supervised learning lies in the availability of a partially observed dataset  $\mathbf{D}_u$ . In much of the imputation literature,  $\mathbf{D}_u$  has traditionally been treated like a test set, i.e., it is not directly used to train  $f$ , and methodological advances have primarily focused on tailoring the function class  $\mathcal{F}$  to specific structures while adhering to the ERM framework in Eq. (1) [7], [10], [14], [27]. For example, convolutional filters are often incorporated for image data, and attention-based Transformer blocks are often used for language data.

Also, access to a partially observed dataset is not unique to imputation. There exist other learning paradigms in this setting. In domain adaptation,  $\mathbf{D}_u$  is interpreted as data drawn from a shifted distribution, and the challenge lies in adapting  $f_l^*$  to this shift [28]. In semi-supervised learning, the problem can be viewed as a special case of imputation where  $\mathbf{z}$  is restricted to one-dimensional features/labels [29].

In this work, we focus on imputation while differentiating it from these related paradigms in two key respects:

- 1) Unlike domain adaptation, the general imputation paradigm assumes that the  $\mathbf{x}$  components in  $\mathbf{D}_l$  and  $\mathbf{D}_u$  are drawn from the same distribution.
- 2) Unlike popular semi-supervised learning methods [30]–[32], the general imputation paradigm does not impose assumptions on, or exploit structural properties of, the target variable  $\mathbf{z}$ .

### B. Measure Consistency Regularization

Intuitively, if a prediction function  $f$  is well learned, the distribution of the imputed version of the partially observed dataset  $\mathbf{D}_u$  should resemble that of the fully observed dataset  $\mathbf{D}_l$ . To promote this similarity, we can leverage a regularization mechanism that enforces consistency between the empirical measures of  $\mathbf{D}_l$  and the imputed version of  $\mathbf{D}_u$ . We refer to this approach as **measure consistency regularization (MCR)**. Formally, MCR augments the ERM objective in Eq. (1) with an additional regularization term as

$$f_u^* = \operatorname{arginf}_{f \in \mathcal{F}} \{\pi_l \mathcal{L}^f + \lambda_d r(\pi_l, \pi_u^f)\}, \quad (2)$$

where  $r(\cdot, \cdot)$  denotes a discrepancy measure between two probability distributions, and  $\lambda_d$  is a tuning parameter controlling the strength of regularization. Note that the subscript in  $f_u^*$  emphasizes the use of the partially observed data  $\mathbf{D}_u$  in training. Under specific loss and discrepancy measure design, the general form (2) recovers several empirically successful

(a) Training with fully observed data in  $\mathcal{L}$  only      (b) Training with  $\mathcal{L} + \text{MCR}$  (NND)

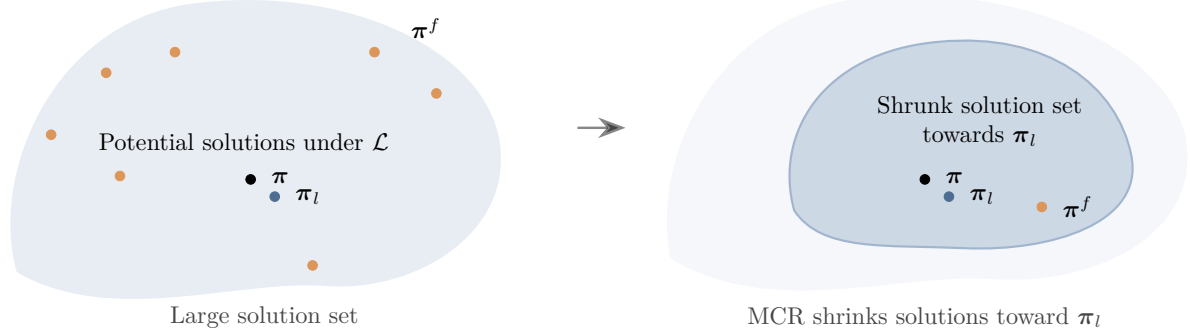


Fig. 1. An intuitive illustration of the effect of measure consistency regularization (MCR). Without MCR, minimizing the supervised loss on the fully observed empirical measure  $\pi_l$  admits a large set of solutions, making the imputed measure induced by the learned function likely to deviate from the true measure  $\pi$ . By enforcing MCR, the learning process encourages the imputed measure to align with  $\pi_l$ , thereby shrinking the solution set and increasing the likelihood that the imputed measure remains close to the true measure.

training schemes for imputation [22], [23] and semi-supervised learning [26], [33].

Discrepancy measures between probability distributions are most commonly drawn from two broad families: integral probability metrics (IPMs) and  $f$ -divergences. Notable IPMs include the Wasserstein distance, maximum mean discrepancy (MMD), and total variation distance, while prominent  $f$ -divergences include the Kullback–Leibler divergence, Jensen–Shannon divergence, and Hellinger distance.

Figure 1 provides a high-level overview of the intuition behind MCR. Without MCR, minimizing the supervised loss on the fully observed empirical measure  $\pi_l$  admits a large set of solutions, making the imputed measure induced by the learned function likely to deviate from the true measure  $\pi$ . By enforcing MCR, the learning process encourages the imputed measure to align with  $\pi_l$ , thereby shrinking the solution set and increasing the likelihood that the imputed measure remains close to the true measure.

### C. Neural Net Distance for MCR

In this work, we focus on the IPM family for measure consistency regularization. The IPM defines a distance between two probability measures  $\mu$  and  $\nu$  with respect to a function class  $\mathcal{G}$  as

$$\text{IPM}_{\mathcal{G}}(\mu, \nu) := \sup_{g \in \mathcal{G}} |\mu g - \nu g|.$$

Several well-known probability metrics are recovered as special cases of IPM: kernel maximum mean discrepancy (MMD) when  $\mathcal{G}$  is a reproducing kernel Hilbert space (RKHS) [34], the 1–Wasserstein distance when  $\mathcal{G}$  is the set of 1–Lipschitz functions [35], and the total variation distance when  $\mathcal{G}$  consists of indicator functions [36, Chapter 3].

Compared to the other widely used class of  $f$ -divergences, IPMs possess several desirable properties. They are bounded, symmetric [37], and robust under support mismatch [38]. Moreover, IPMs can often be computed with linear complexity in the number of samples. This contrasts with certain optimal

transport metrics closely related to IPMs, such as the quadratic-cost Wasserstein distance [39], Sinkhorn distance [23], and masked optimal transport (MOT) [24], whose computational costs typically scale quadratically with sample size.

Despite these advantages, direct computation of IPMs can be difficult because the function class  $\mathcal{G}$  rarely yields analytical solutions. Neural net distance (NND) provides a practical surrogate by restricting  $\mathcal{G}$  to neural network architectures [25]. Specifically, the distance between measures  $\mu$  and  $\nu$  is defined as

$$d_{\mathcal{G}_{nn}}(\mu, \nu) := \sup_{g \in \mathcal{G}_{nn}} |\mu g - \nu g|, \quad (3)$$

where  $\mathcal{G}_{nn}$  denotes the class of neural networks. One can show that the above definition automatically follows the properties of metrics such as non-negativity, symmetry, and triangle inequality. Moreover, it is discriminative, i.e.,  $R(f) = 0$  if and only if  $\pi = \pi^f$  for sufficiently rich  $\mathcal{G}_{nn}$  (e.g., RKHS unit ball with characteristic kernel, Lipschitz functions) [40], therefore making it a proper distance metric as well. The maximization problem in Eq. (3) is typically solved with gradient-based optimization. In the context of Generative Adversarial Networks (GANs), the function  $g$  is often interpreted as the discriminator [38], [41].

The neural net distance thus defines an optimization-friendly metric that integrates seamlessly into the MCR framework in Eq. (2). The resulting formulation is

$$f_u^* = \operatorname{arginf}_{f \in \mathcal{F}} \{ \pi_l \mathcal{L}^f + \lambda_d d_{\mathcal{G}_{nn}}(\pi_l, \pi_u^f) \}, \quad (4)$$

where  $d_{\mathcal{G}_{nn}}$  is defined in Eq. (3) with  $g \in \mathcal{G}_{nn} : \mathcal{X} \times \mathcal{Z} \rightarrow \mathbb{R}$ , and  $\lambda_d$  controls the strength of the regularization.

In the remainder of this work, we develop our theoretical analysis specifically for MCR with neural net distance, owing to its generality, flexibility, and practical tractability.

## III. LITERATURE REVIEW

**I) Measure Consistency Regularization:** There exist several strands of literature that employ the idea of enforcing measure

consistency between the imputed data and observed data. For example, [22] propose to use discriminators to differentiate the observed and imputed portion of each data point. [21] further introduce observed data supervision to the work of [22]. [23], [24], [39] use second-order optimal transport to enforce the measure consistency.

Moreover, there also exists a rich measure consistency regularization literature in the SSL community that seeks to align labeled and unlabeled data through various conformity enforcing mechanism. However, most of these approaches rely heavily on the premise of scalar or simplex outputs [30]–[32]. There exists a line of work that specifically enforces measure consistency with optimal transport and integral probability metric [26], [42], which be viewed as a special case of imputation with measure consistency regularization via integral probability metric, where the imputed value is a scalar label.

Most importantly, we note that all the aforementioned works are only empirically evaluated in specific domains, and the theoretical understanding of their practical success has remained elusive.

**II) Neural Net Distance:** Neural net distance, introduced in [25], is an approximation to integral probability metrics (IPMs), where one uses a class of neural networks as discriminators to measure discrepancy between two distributions. Since then, it has been used extensively in generative adversarial frameworks [38], [41]. Theoretical analyses have examined (i) the convergence of empirical neural-net distances to the true population IPM under capacity constraints [25], [43], and (ii) generalization in GANs—i.e. how small neural-net distance between generated and true distributions implies closeness in some other statistical sense [40], [44], [45].

Beyond generation, neural-net distance (and more generally, IPMs) are natural regularizers for imputation/predictive tasks [46], [47]: if one imputes missing features, requiring that the imputed data distribution be close under some neural net distances to that of the fully observed data can help enforce plausible imputations. While many works use adversarial losses (GANs) or discriminators in this spirit (for example GAIN [22]), few have explicitly used neural-net or IPM theory to understand when such regularization helps in imputation.

In light of these, our contribution leverages neural-net distance / IPM-style regularization as part of a *unifying, domain-agnostic* theoretical framework for measure consistency regularization. We aim to show under what conditions such regularizers guarantee better imputation, not just empirically (as many prior works do), and how this applies across modalities (tabular, image, multi-modal etc.)

**III) Imputation in Modern Landscape:** Our target problem formulation is inline with imputation tasks under structured missingness [12], [18] from a mathematical standpoint. It is more commonly referred to as cross-modal or multi-modal imputation [7], [8], [10], [11], [24] in recent literature, where the missingness happens to a specific data modality. Single cell data analysis is one of the most active communities studying imputation problems, mainly due to profiling technology limitations. Most of the recent advancement in single cell data imputation lies on the modification of the latent space in variational autoencoders [13]–[15], [17], [48], [49]. However,

all of the techniques only use information from the fully observed dataset in learning the prediction function, and they do not take advantage of the partially observed dataset.

We note that there exist a number of studies that successfully incorporate the partially observed data with measure consistency regularization. [21], [22] use discriminators to force the generators to impute believable data for partially observed data. [23], [24], [39] apply optimal transport to enforce measure consistency between observed data and imputed data, the complexity of which scales quadratically with respect to the number of fully observed and partially observed data.

#### IV. ON THE GENERALIZATION BENEFIT OF MCR

We analyze generalization strictly in terms of NND, a common choice for literature in domain adaptation and generative modeling [25], [40], [43]–[45], [50]. Specifically, we define the generalization error  $R(f)$  of a prediction function  $f : \mathcal{X} \rightarrow \mathcal{Z}$  with respect to the NND function class  $g \in \mathcal{G}_{nn}$  as

$$R(f) = d_{\mathcal{G}_{nn}}(\boldsymbol{\pi}, \boldsymbol{\pi}^f) = \sup_{g \in \mathcal{G}_{nn}} |\boldsymbol{\pi}g - \boldsymbol{\pi}^f g|. \quad (5)$$

Since MCR does not alter the architecture of the prediction model (i.e., the function class  $\mathcal{F}$ ), the best achievable generalization error is always  $\inf_{f \in \mathcal{F}} d_{\mathcal{G}_{nn}}(\boldsymbol{\pi}, \boldsymbol{\pi}^f)$  [44]. Consequently, the key quantity of interest is the *estimation error*, defined for a learned function  $\hat{f}$  as

$$R(\hat{f}) - \inf_{f \in \mathcal{F}} R(f) = d_{\mathcal{G}_{nn}}(\boldsymbol{\pi}, \boldsymbol{\pi}^{\hat{f}}) - \inf_{f \in \mathcal{F}} d_{\mathcal{G}_{nn}}(\boldsymbol{\pi}, \boldsymbol{\pi}^f), \quad (6)$$

which quantifies the gap MCR seeks to reduce.

##### A. Perfect Training

We first derive the estimation error bound under perfect training, where the learned function exactly minimizes the corresponding loss functions in Eq. (1) and Eq. (4). We impose the following assumptions.

**Assumption 1.** *The feature space  $\mathcal{X}$  and target space  $\mathcal{Z}$  are bounded with sizes  $B_x$  and  $B_z$ , respectively, and the joint space by  $B_{xz}$ . Accordingly, prediction functions  $f : \mathcal{X} \rightarrow \mathcal{Z}$  are bounded by  $B_z$ . In addition, all neural distance functions  $g \in \mathcal{G}_{nn}$  are assumed to be Lipschitz continuous with constant at most  $B_g$  within a symmetric class  $\mathcal{G}_{nn}$  ( $g \in \mathcal{G}_{nn} \Leftrightarrow -g \in \mathcal{G}_{nn}$ ). The size of a space is defined with respect to  $\|\cdot\|_2$ .*

We note that the above assumptions apply to almost any existing neural network (with bounded weights after training [51]) and finite datasets [52]. Since we focus on the perfect training case in this section, we also impose the following mild assumptions.

**Assumption 2.** *Let  $\mathcal{F}_1 = \{f : f = \operatorname{arginf}_{f \in \mathcal{F}} \mathcal{L}^f\}$  denote the minimizer set of the prediction loss on fully observed data, and  $\mathcal{F}_2 = \{f : f = \operatorname{arginf}_{f \in \mathcal{F}} d_{\mathcal{G}_{nn}}(\boldsymbol{\pi}_l, \boldsymbol{\pi}_l^f)\}$  the minimizer set of the NND loss. We assume perfect fit exists on  $\mathbf{D}_l$ , such that  $\mathcal{F}_1 = \mathcal{F}_2 = \mathcal{F}^*$ , where  $\mathcal{F}^* = \{f : \mathbf{z} = f(\mathbf{x}), \forall (\mathbf{x}, \mathbf{z}) \in \mathbf{D}_l\}$ .*

**Assumption 3.** *Let  $\mathcal{F}_3 = \{f : f = \operatorname{arginf}_{f \in \mathcal{F}} d_{\mathcal{G}_{nn}}(\boldsymbol{\pi}_l, \boldsymbol{\pi}_u^f)\}$  denote the minimizer set on the imputed partially observed data, and  $\mathcal{F}_4 = \{f : f = \operatorname{arginf}_{f \in \mathcal{F}} d_{\mathcal{G}_{nn}}(\boldsymbol{\pi}_l, \boldsymbol{\pi}_{ul}^f)\}$  denote the*

minimizer set on the imputed mixture of fully and partially observed datasets (both imputed by function  $f$ ). We assume that  $\mathcal{F}^* \cap \mathcal{F}_3 \neq \emptyset$  and  $\mathcal{F}^* \cap \mathcal{F}_4 \neq \emptyset$ .

These conditions are mild and common in interpolation study for sufficiently expressive hypothesis classes  $\mathcal{F}$  [53]. For example, Assumption 2 holds when  $\mathcal{F}$  is flexible enough to interpolate  $\mathbf{D}_l$ , while Assumption 3 can be ensured if  $\mathcal{F}$  allows perfect fitting of  $\mathbf{D}_l$  even under MCR. We now present the main result of this section.

**Theorem 1.** Suppose Assumptions 1–3 hold. Let  $\hat{\mathfrak{R}}_n(\mathcal{G}_{nn})$  denote the Rademacher complexity of  $\mathcal{G}_{nn}$  on  $n$  samples, and let  $\mathcal{H} := \{h(\mathbf{x}) = g(\mathbf{x}, f(\mathbf{x})) : g \in \mathcal{G}_{nn}, f \in \mathcal{F}\}$ . Then,

- 1) For a function  $f_l^* \in \mathcal{F}$  learned with  $n$  fully observed samples without MCR (Eq. (1)), the estimation error in Eq. (6) is bounded with probability at least  $1 - 2\delta$  as

$$R(f_l^*) - \inf_{f \in \mathcal{F}} R(f) \leq 4\hat{\mathfrak{R}}_n(\mathcal{G}_{nn}) + 4\hat{\mathfrak{R}}_n(\mathcal{H}) + \frac{2\Delta}{\sqrt{n}},$$

where  $\Delta = 3B_g B_{xz} \sqrt{2 \ln \delta^{-1}}$ .

- 2) For a function  $f_u^* \in \mathcal{F}$  learned with  $n$  fully observed and  $m$  partially observed samples with MCR (Eq. (4)), the estimation error in Eq. (6) is bounded with probability at least  $1 - 2\delta$  as

$$\begin{aligned} R(f_u^*) - \inf_{f \in \mathcal{F}} R(f) &\leq 4\hat{\mathfrak{R}}_n(\mathcal{G}_{nn}) + 4\hat{\mathfrak{R}}_{m+n}(\mathcal{H}) \\ &\quad + \Delta \left( \frac{1}{\sqrt{n}} + \frac{1}{\sqrt{m+n}} \right). \end{aligned}$$

Theorem 1 establishes that MCR improves the estimation error bound for any bounded prediction function. The improvement does not alter the asymptotic rate with respect to  $n$ , which is order-wise in line with well-established semi-supervised learning results studying specific model choices and loss functions [54], [55]. However, as oppose to the existing results in semi-supervised learning, our theory suggests the benefits in terms of NND when  $m \gg n$  exists for a much broader class of output structure, model hypothesis, and loss functions. For specific model architectures like neural networks with bounded spectral norms, we can also obtain concrete upper bound by upper bounding the empirical Rademacher complexity following the proof in [56], thereby yielding a concrete upper bound on the estimation error.

## B. Imperfect Training

In the previous subsection, we analyzed the impact of MCR on the estimation error under the assumption of perfect training. In practice, however, the non-convex optimization landscape and the large hypothesis class often prohibit the convergence to a global minima, leaving a non-zero optimality gap. We therefore extend our analysis to the imperfect training case, where  $\pi_l \mathcal{L}^{f_l} > 0$ , where  $f_l$  is a function learned through solving (1) with a numerical solver. Our goal is to extend the previous theoretical results to this practical scenario to later provide algorithmic insights on handling the optimality gap (Section V) and demonstrate the potential benefit from training with MCR.

To this end, we first introduce a notion of *loss function dominance*, which describes bounding relationships between different loss functions.

**Definition 1.** Given two loss functions  $\mathcal{L}$  and  $\mathcal{R}$  defined on the same dataset  $\mathbf{D} : \{(\mathbf{x}_i, \mathbf{z}_i)\}_{i=1}^n \in (\mathcal{X}, \mathcal{Z})^n\}$  (with empirical distribution  $\pi$ ) and a prediction function  $f$ , we say that  $\mathcal{L}$  is  $(C, \alpha)$ -dominated by  $\mathcal{R}$  if

$$\pi \mathcal{L} \leq C(\pi \mathcal{R})^\alpha,$$

for some constants  $C, \alpha \in \mathbb{R}^+$ , for  $\forall \mathbf{D} \in (\mathcal{X}, \mathcal{Z})^n$  and  $\forall f \in \mathcal{F}$ .

The definition is akin to popular bounding relationships between probability metrics [57] and Hölder equivalence in metric studies [58], [59], extended towards general loss functions. This dominance notion is asymmetric:  $\mathcal{L}$  being  $(C, \alpha)$ -dominated by  $\mathcal{R}$  does not imply the reverse. When  $\mathcal{R}$  is a distance metric in Euclidean space, this definition resembles classical smoothness conditions such as Lipschitz or Hölder continuity. Although NND is not a simple instance-wise expectation, it still qualifies as a loss function defined over a dataset, enabling us to connect it to common loss functions under this framework.

Table I illustrates how choices of the neural distance class  $\mathcal{G}_{nn}$  yield NNDs that are  $(C, \alpha)$ -dominated by standard loss functions. A derivation for the associated  $(C, \alpha)$  values is provided in the supplementary materials. This motivates the following condition under imperfect training.

**Assumption 4.** We assume that the primary loss function  $\mathcal{L}$  in Eq. (4) is non-negative with minimum value of 0 for simplicity. The neural distance class  $\mathcal{G}_{nn}$  is chosen such that the induced NND is  $(C, \alpha)$ -dominated by  $\mathcal{L}$ , i.e., for any distribution  $\pi$  and prediction function  $f$ , we have

$$d_{\mathcal{G}_{nn}}(\pi, \pi^f) \leq C(\pi \mathcal{L}^f)^\alpha.$$

Furthermore, imperfect training results in a learned function  $f_l \in \mathcal{F}$  with  $\pi_l \mathcal{L}^{f_l} = \epsilon_{\mathcal{L}} \geq 0$ .

In addition, the MCR framework introduces a potential optimization gap for the regularization term, motivating the following assumption.

**Assumption 5.** For a predictor  $f_u$  learned with MCR and associated neural distance function

$$g_u = \arg \sup_{g \in \mathcal{G}_{nn}} |\pi_l g - \pi_u^{f_u} g|,$$

we assume that  $f_u$  achieves the same optimality gap on  $\mathcal{L}$  as the baseline function  $f_l$ , i.e.,

$$\pi_l \mathcal{L}^{f_u} = \epsilon_{\mathcal{L}} \geq 0,$$

and that the penalty term admits an additional gap defined as

$$\epsilon_d := |\pi_l g_u - \pi_u^{f_u} g_u| - \inf_{f \in \mathcal{F}} d_{\mathcal{G}_{nn}}(\pi_l, \pi_u^f) \geq 0. \quad (7)$$

$\epsilon_d$  in above can be thought as the optimality gap in solving the minimization problem  $d_{\mathcal{G}_{nn}}(\pi_l, \pi_u^f)$  over  $f \in \mathcal{F}$  via a numerical solver. We can now state the estimation error bound in the imperfect training scenario.

TABLE I

NEURAL DISTANCE CLASS  $\mathcal{G}_{nn}$  AND THE COMMON LOSS FUNCTIONS THEY ARE  $C, \alpha$  DOMINATED BY.  $\mathcal{V}$  DENOTES THE REPRODUCING KERNEL HILBERT SPACE WITH FEATURE MAP  $\phi$ .  $\hat{\mathbf{z}} = f(\mathbf{x})$ .  $\mathcal{L}_{NLL}$  DENOTE THE EXCESS NEGATIVE LOG-LIKELIHOOD LOSS.

Loss $\mathcal{L}$ (Omitting Expectation)	Neural Distance Class $\mathcal{G}_{nn}$	$C, \alpha$
$\mathcal{L}_1(\mathbf{z}, \hat{\mathbf{z}}) = \ \mathbf{z} - \hat{\mathbf{z}}\ _1$	$\mathcal{G}_{nn} = \{g : g \text{ is 1-Lipschitz}\}$	1, 1
$\mathcal{L}_2(\mathbf{z}, \hat{\mathbf{z}}) = \ \mathbf{z} - \hat{\mathbf{z}}\ _2^2$	$\mathcal{G}_{nn} = \{g : g \text{ is 1-Lipschitz}\}$	1, 1/2
$\mathcal{L}_{NLL}(\hat{\mathbf{z}}, \mathbf{z}) = -\log q_f(\hat{\mathbf{z}} \mathbf{x}) + \log p(\mathbf{z} \mathbf{x})$	$\mathcal{G}_{nn} = \{g : \ g\ _\infty \leq 1\}$	$\sqrt{2}, 1/2$
$\mathcal{L}_{\mathcal{V}}(\mathbf{z}, \hat{\mathbf{z}}) = \ \phi(\mathbf{z}) - \phi(\hat{\mathbf{z}})\ _{\mathcal{V}}^2$	$\mathcal{G}_{nn} = \{g \in \mathcal{V} : \ g\ _{\mathcal{V}} \leq 1\}$	1, 1/2

**Theorem 2.** Suppose Assumptions 1-5 hold. Using the same notation as in Theorem 1, we obtain:

1) For  $f_l \in \mathcal{F}$  trained on  $n$  fully observed samples without MCR, the estimation error is bounded with probability at least  $1 - 2\delta$  as

$$R(f_l) - \inf_{f \in \mathcal{F}} R(f) \leq 4\hat{\mathfrak{R}}_n(\mathcal{G}_{nn}) + 4\hat{\mathfrak{R}}_n(\mathcal{H}) + \frac{2\Delta}{\sqrt{n}} + C(\epsilon_{\mathcal{L}})^\alpha, \quad (8)$$

where  $\Delta = 3B_g B_{xz} \sqrt{2 \ln \delta^{-1}}$ , and constants  $C, \alpha$  are results of loss function dominance.

2) For  $f_u \in \mathcal{F}$  trained on  $n$  fully observed and  $m$  partially observed samples with MCR, the estimation error is bounded with probability at least  $1 - 2\delta$  as

$$R(f_u) - \inf_{f \in \mathcal{F}} R(f) \leq 4\hat{\mathfrak{R}}_n(\mathcal{G}_{nn}) + 4\hat{\mathfrak{R}}_{m+n}(\mathcal{H}) + \Delta\left(\frac{1}{\sqrt{n}} + \frac{1}{\sqrt{m+n}}\right) + \frac{n}{m+n}C(\epsilon_{\mathcal{L}})^\alpha + \frac{m}{m+n}(\epsilon_d + 2\xi), \quad (9)$$

where  $\xi := \inf_{f \in \mathcal{F}} d_{\mathcal{G}_{nn}}(\boldsymbol{\pi}_l, \boldsymbol{\pi}_u^f)$ .

Compared with Theorem 1, imperfect training introduces three additional error terms:  $C(\epsilon_{\mathcal{L}})^\alpha$  from the suboptimality of the training loss,  $\epsilon_d$  from the suboptimality of the penalty term, and  $\xi$  from the sampling discrepancy between the fully observed and partially observed datasets. While the first overhead is unavoidable and appears regardless of MCR, the term  $\epsilon_d$  and  $\xi$  obscures the theoretical advantage of MCR. This difficulty is inherent to min-max optimization problems and the random sampling process. Nevertheless, we argue that in practice the  $\epsilon_d$  term is recoverable, and in the next section we propose strategies to mitigate it, thereby restoring the robustness benefits of MCR.

## V. HANDLING THE OPTIMALITY GAP

In this section, we develop a practical framework to manage the optimality gap  $\epsilon_d$ . From a robustness perspective, MCR offers an advantage over vanilla training only when  $\epsilon_d$  is sufficiently small, such that the right-hand side (RHS) of Eq. (8) is larger than that of Eq. (9). In other words, the robustness of MCR is preserved with high probability when

$$\frac{m}{m+n}(\epsilon_d + 2\xi - C(\epsilon_{\mathcal{L}})^\alpha) \leq 4(\hat{\mathfrak{R}}_n(\mathcal{H}) - \hat{\mathfrak{R}}_{m+n}(\mathcal{H})) + \Delta\left(\frac{1}{\sqrt{n}} - \frac{1}{\sqrt{m+n}}\right). \quad (10)$$

One straightforward way to guarantee robustness is to penalize the MCR term heavily, ensuring  $\epsilon_d \leq C(\epsilon_{\mathcal{L}})^\alpha$ . However, imposing a large  $\lambda_d$  may hinder convergence on  $\mathcal{L}$ , violating Assumption 5. This raises the practical question: under what conditions can robustness still be ensured with a moderate choice of  $\lambda_d$  that prioritizes minimizing  $\mathcal{L}$ ? To answer this, we further analyze the RHS of Eq. (10).

The Rademacher complexity is generally difficult to estimate in practice, but the robustness of MCR is still guaranteed under the simplified condition

$$\frac{m}{m+n}(\epsilon_d + 2\xi - C(\epsilon_{\mathcal{L}})^\alpha) \leq \Delta\left(\frac{1}{\sqrt{n}} - \frac{1}{\sqrt{m+n}}\right), \quad (11)$$

which is in fact tighter, because  $\hat{\mathfrak{R}}_n(\mathcal{H})$  is usually larger than  $\hat{\mathfrak{R}}_{m+n}(\mathcal{H})$  when  $m$  is large. The remaining constant  $\Delta$  is relatively easy to estimate:  $B_{xz}$  can be approximated by the maximum pairwise distance in the data, while  $B_g$  depends on the neural distance class  $\mathcal{G}_{nn}$ . This often yields a conservative estimate  $\hat{\Delta}$ , which further guarantees the robustness.

In practice, empirically estimating  $\xi$  via IPM could potentially be unstable, especially for flexible function classes  $\mathcal{F}$  and distance measures such as Wasserstein-type IPMs in moderate to high dimensions. Even when two empirical distributions are generated from the same underlying population, the resulting empirical IPM is typically non-negligible due to finite-sample variability and estimator bias. As a consequence, a naive plug-in estimate of  $\xi$  may substantially overstate the effective distributional discrepancy and lead to overly pessimistic conclusions in the decision condition (11).

To address this issue, we adopt a calibrated discrepancy estimation strategy that explicitly accounts for the intrinsic fluctuation in IPM calculations. First, we approximate  $\xi$  by the marginal discrepancy in the  $\mathbf{x}$  component,

$$\xi \approx d_{\mathcal{G}_{nn}}(\boldsymbol{\pi}_l(\mathbf{x}), \boldsymbol{\pi}_u(\mathbf{x})),$$

with a slight abuse of notation. We note that this is a crude and conservative ( $d_{\mathcal{G}_{nn}}(\boldsymbol{\pi}_l(\mathbf{x}), \boldsymbol{\pi}_u(\mathbf{x})) \leq \xi$  in theory) approximation aiming at simplifying the estimation process by ruling out the effect of  $f \in \mathcal{F}$ .

To isolate the excess discrepancy attributable to distribution shift, we estimate the IPM noise floor by exploiting the fact that subsets drawn from the fully observed dataset  $\mathbf{D}_l$  share the same generating distribution. Specifically, we propose the following procedure:

- 1) Sample multiple random subsets from  $\mathbf{D}_l$  with sizes matched to those used in the labeled-unlabeled comparison.

- 2) Compute the average IPM estimate between the  $\mathbf{x}$  components of these subsets, denoted by  $d_l$ .
- 3) Define the calibrated discrepancy as

$$\hat{\xi} := \max \left\{ d_{\mathcal{G}_{nn}}(\boldsymbol{\pi}_l(\mathbf{x}), \boldsymbol{\pi}_u(\mathbf{x})) - d_l, 0 \right\}. \quad (12)$$

The quantity  $d_l$  serves as an empirical baseline capturing the intrinsic IPM variability under the null hypothesis of no distribution shift. By subtracting this baseline,  $\hat{\xi}$  measures the excess discrepancy beyond what would be expected solely from finite-sample effects. Importantly, we do not claim that  $\hat{\xi}$  is an unbiased or consistent estimator of the population IPM; rather, it is a calibrated statistic tailored to the finite-sample decision-making role of Condition (11).

The remaining task is to characterize  $\epsilon_d$  itself. Recall that  $\epsilon_d$  is defined as the optimality gap of the penalty term in Eq. (7). To study it, we leverage the notion of *duality gap* in min-max optimization. For a general min-max problem

$$\inf_{f \in \mathcal{F}} \sup_{g \in \mathcal{G}} \mathcal{L}(f, g),$$

the *duality gap* for a pair  $(\hat{f}, \hat{g})$  is defined as

$$DG(\hat{f}, \hat{g}) := \sup_{g \in \mathcal{G}} \mathcal{L}(\hat{f}, g) - \inf_{f \in \mathcal{F}} \mathcal{L}(f, \hat{g}).$$

Duality gap has been widely adopted as a practical convergence indicator for min-max problems, especially in generative adversarial training [60]–[62]. Here, we employ it as a proxy to monitor and bound the optimality gap  $\epsilon_d$ .

**Theorem 3.** For  $f_u \in \mathcal{F}$  and  $g_u \in \mathcal{G}_{nn}$  as defined in Assumption 5, the duality gap

$$DG(f_u, g_u) := \sup_{g \in \mathcal{G}_{nn}} |\boldsymbol{\pi}_l g - \boldsymbol{\pi}_u^{f_u} g| - \inf_{f \in \mathcal{F}} |\boldsymbol{\pi}_l g_u - \boldsymbol{\pi}_u^f g_u|,$$

upper bounds the optimality gap  $\epsilon_d$  defined in Eq. (7) as follows

$$\epsilon_d \leq DG(f_u, g_u).$$

*Proof.* Let  $d\omega(f, g) = |\boldsymbol{\pi}_l g - \boldsymbol{\pi}_u^f g|$ . We aim to show

$$\begin{aligned} d\omega(f_u, g_u) - \inf_{f \in \mathcal{F}} \sup_{g \in \mathcal{G}_{nn}} d\omega(f, g) \\ \leq \sup_{g \in \mathcal{G}_{nn}} d\omega(f_u, g) - \inf_{f \in \mathcal{F}} d\omega(f, g_u). \end{aligned}$$

Observe that

$$\begin{aligned} d\omega(f_u, g_u) &= \sup_{g \in \mathcal{G}_{nn}} d\omega(f_u, g), \\ \inf_{f \in \mathcal{F}} \sup_{g \in \mathcal{G}_{nn}} d\omega(f, g) &\geq \inf_{f \in \mathcal{F}} d\omega(f, g_u), \end{aligned}$$

where the first line follows from the definition of  $g_u$ . Combining the two inequalities completes the proof.  $\square$

Theorem 3 shows that we do not need to compute  $\epsilon_d$  directly, which is difficult to evaluate, but can instead monitor the duality gap during training. As training progresses, a small duality gap indicates that the neural distance function and predictor are nearly at equilibrium, ensuring that  $\epsilon_d$  is also small enough to preserve the robustness benefit of MCR.

**Corollary 4.** For predictors  $f_u$  and  $f_l$  trained with and without MCR down to the same training error  $\epsilon_{\mathcal{L}}$ , and neural distance

function  $g_u$ , the robustness benefit of MCR holds with high probability whenever

$$DG(f_u, g_u) \leq \hat{\Delta} \frac{m + n - \sqrt{(m + n)n}}{m\sqrt{n}} + C(\epsilon_{\mathcal{L}})^{\alpha} - 2\hat{\xi}. \quad (13)$$

Also, if the  $\hat{\Delta}$  and  $\hat{\xi}$  estimates from the dataset yield the following identity

$$\hat{\Delta} \frac{m + n - \sqrt{(m + n)n}}{m\sqrt{n}} < 2\hat{\xi}, \quad (14)$$

then MCR training is no longer practically beneficial, at least in well trained regimes where  $\epsilon_{\mathcal{L}} \rightarrow 0$ .

---

**Algorithm 1** Batch MCR Training with Duality Gap Stopping Condition

---

**Require:**  $f_{\theta}$ ,  $g_{\gamma}$ ,  $\mathbf{D}_l$ ,  $\mathbf{D}_u$ , an estimated  $\hat{\Delta}$  and  $\hat{\xi}$ , loss  $\mathcal{L} : \mathcal{X} \times \mathcal{Z} \rightarrow \mathbb{R}$ , Optimizer  $O$ , MCR update step  $n_g$ , Duality Gap update step  $n_d$ , MCR weight  $\lambda_d$ ,  $\theta$  learning rate  $\alpha_{\theta}$  and convergence criterion,  $\gamma$  learning rate  $\alpha_{\gamma}$ ,  $\tau = \text{True}$ .

**While:**  $\theta$  does not converge or  $\tau$ :

```

1: procedure MCR TRAINING( $\theta$ )
2:   Divide  $\mathbf{D}_l$  into  $k_l$  batches
3:   for  $i \leftarrow 1$  to  $k_l$  do
4:     for  $t \leftarrow 1$  to  $n_g$  do
5:       Divide  $\mathbf{D}_u$  into  $k_u$  batches
6:       for  $j \leftarrow 1$  to  $k_u$  do
7:          $d_j = \boldsymbol{\pi}_u^{f_{\theta}, j} g_{\gamma} - \boldsymbol{\pi}_l^j g_{\gamma}$ 
8:       end for
9:        $\gamma \leftarrow O\left(\frac{1}{k_u} \sum d_j; \alpha_{\gamma}\right)$ 
10:      end for
11:       $\theta \leftarrow O\left(\boldsymbol{\pi}_l^i \mathcal{L} - \lambda_d \boldsymbol{\pi}_u^{f_{\theta}, j} g_{\gamma}; \alpha_{\theta}\right)$ 
12:    end for
13:    if  $\theta$  converges then
14:       $\gamma' = \gamma$ ,  $\theta' = \theta$ , record  $\epsilon_{\mathcal{L}}$ 
15:      for  $q \leftarrow 1$  to  $n_d$  do
16:        Get a random batch  $\boldsymbol{\pi}_l$  and  $\boldsymbol{\pi}_u$ 
17:         $d_q = \boldsymbol{\pi}_u^{f_{\theta}} g_{\gamma'} - \boldsymbol{\pi}_l g_{\gamma'}$ 
18:         $d'_q = \boldsymbol{\pi}_u^{f_{\theta'}} g_{\gamma} - \boldsymbol{\pi}_l g_{\gamma}$ 
19:         $\gamma' \leftarrow O(d_q; \alpha_{\gamma})$ 
20:         $\theta' \leftarrow O(-d'_q; \alpha_{\theta})$ 
21:      end for
22:      Sample a large batch  $\boldsymbol{\pi}_l$  and  $\boldsymbol{\pi}_u$ 
23:       $d = \boldsymbol{\pi}_u^{f_{\theta}} g_{\gamma'} - \boldsymbol{\pi}_l g_{\gamma'}$ 
24:       $d' = \boldsymbol{\pi}_u^{f_{\theta'}} g_{\gamma} - \boldsymbol{\pi}_l g_{\gamma}$ 
25:      if  $d' - d \leq \text{RHS}$  of Eq. (13) then
26:         $\tau = \text{False}$ 
27:      else
28:         $\tau = \text{True}$ 
29:      end if
30:    end if
31:  end procedure

```

---

Corollary 4 follows from Theorem 3 and Eq. (11), yielding an explicit analytical bound that can be used as a stopping condition for MCR training. Moreover, it provides an identification approach to warn against adopting MCR training when

TABLE II

RECONSTRUCTION ERROR REDUCTION PERCENTAGE (%) WITH MCR. ON COLUMNS TITLE, WE HAVE THE NUMBER OF FULLY OBSERVED DATA  $n$ . ON ROWS TITLE, WE HAVE THE RATIO  $m/n$ . STATISTICALLY SIGNIFICANT REDUCTIONS (COMPARED TO ZERO AS BENCHMARK) ARE DENOTED IN **bold**.

$m/n \backslash n$	10	25	50	100	200
2	$0.79 \pm 0.94$	$-0.37 \pm 0.49$	<b><math>2.25 \pm 0.61</math></b>	<b><math>2.97 \pm 0.61</math></b>	<b><math>2.72 \pm 0.4</math></b>
10	$0.46 \pm 0.47$	$0.24 \pm 0.49$	<b><math>3.3 \pm 0.41</math></b>	<b><math>2.89 \pm 0.42</math></b>	<b><math>2.88 \pm 0.34</math></b>
20	<b><math>0.76 \pm 0.69</math></b>	<b><math>2.1 \pm 0.44</math></b>	<b><math>3.6 \pm 0.38</math></b>	<b><math>4.26 \pm 0.5</math></b>	<b><math>3.71 \pm 0.36</math></b>

there exist significant discrepancy between the fully observed and partially observed dataset (i.e., large  $\xi$ ), which pushes the learning problem into domain adaptation territory.

Next, we translate this result into the practical MCR training protocol summarized in Algorithm 1, which incorporates a duality-gap based stopping criterion. Algorithm 1 presents a generic MCR training framework, with particular emphasis on the stopping mechanism. The central idea is to monitor the magnitude of the duality gap after the predictor parameters  $\theta$  have converged, and to continue training until this gap becomes sufficiently small, as characterized in Corollary 4. We emphasize that the stopping condition is derived by comparing high-probability upper bounds on the estimation error under vanilla training and MCR training. Consequently, satisfying the condition guarantees robustness improvements relative to vanilla training, but does not directly imply improved generalization. Nevertheless, as shown in our simulation studies, the proposed stopping criterion also provides a reliable empirical indicator of stronger generalization performance, even in the absence of explicit model validation.

**Remark 1.** We provide several clarifications regarding Algorithm 1:

- 1) Only in Algorithm 1, we use  $\pi_u^{f_\theta, j} g_\gamma$  to denote expectation of  $g_\gamma$  over the empirical distribution of the  $j$ -th batch partially observed dataset imputed with prediction function  $f_\theta$ . Note that during the  $\theta$  update, the regularization is enforced with the  $j$ -th batch of the partially observed data where  $j = k_u$ , a common practice in adversarial training [41].
- 2) In practice, extending training time typically ensures the stopping condition is satisfied. Thus, the algorithm primarily acts as a safeguard, guaranteeing robustness even under limited computational budgets.
- 3) In specific cases, additional constraints may need to be incorporated. For example, when employing the 1-Wasserstein distance, it is necessary to enforce the 1-Lipschitz constraint. This can be achieved by augmenting the MCR training process with a gradient penalty term [41].

## VI. SIMULATIONS

We now present simulation results. For MCR training, we focus on the first-order Wasserstein distance as the regularization metric. This choice is motivated by its popularity among IPMs, its stability in gradient-based training [38], and its optimization-friendly implementation with gradient penalties [41]. In this case, the neural net distance is defined with  $\mathcal{G}$  as the class

of 1-Lipschitz functions, and we adopt the gradient penalty strategy of [41].

All implementation details—including model architecture, hyperparameter settings, data preprocessing, and optimizers—are provided in the supplementary materials for reproducibility. Each simulation is repeated for 20 Monte Carlo runs to compute error bars.

### A. Verifying Theoretical Claims

We begin with ablation studies on a synthetic dataset to examine the theoretical claims. The target  $\mathbf{z}$  is generated by transforming  $\mathbf{x}$  through a randomly initialized multilayer perceptron (MLP), with  $\mathbf{x} \sim \mathcal{N}(0, I_{30})$  and  $\mathbf{z} \in \mathbb{R}^{20}$ . We evaluate the reconstruction error reduction percentage:

$$\frac{\text{RMSE}(\mathbf{z}, f_l^*(\mathbf{x})) - \text{RMSE}(\mathbf{z}, f_u^*(\mathbf{x}))}{\text{RMSE}(\mathbf{z}, f_l^*(\mathbf{x}))} \times 100\%,$$

where  $f_l^*$  is learned by pure supervision (Eq. (1)) and  $f_u^*$  by MCR (Eq. (4)). Here, RMSE denotes root mean squared error, and higher percentages indicate greater improvements from MCR. Models in this subsection are selected using validation error.

*Interplay between fully and partially observed data ( $n$  and  $m$ ):* A central quantity in our theoretical bounds (Theorems 1 and 2) is the difference

$$\Delta \left( \frac{1}{\sqrt{n}} - \frac{1}{\sqrt{m+n}} \right),$$

which captures how additional partially observed samples reduce the estimation error relative to pure supervision. This expression suggests two effects: (i) for fixed  $n$ , increasing  $m$  should amplify the benefit of MCR; and (ii) for fixed  $m/n$ , larger  $n$  should make this advantage more pronounced, as other error components diminish.

To test this prediction, we fix the data-generating distribution and use a two-hidden-layer MLP as the predictor class  $\mathcal{F}$ , while varying  $n \in \{10, \dots, 200\}$  and the ratio  $m/n \in \{2, 10, 20\}$ . The resulting reconstruction error reductions are summarized in Table II. When  $n$  is small, a large  $m$  is required to obtain statistically significant improvements, reflecting the dominance of the  $1/\sqrt{n}$  generalization term and the resulting high variance among empirically optimal predictors. As  $n$  increases, MCR yields more stable and consistent gains, with improvements scaling predictably with  $m/n$ , in agreement with Theorem 1.

*Role of model capacity and approximation error.:* Our analysis separates estimation error into generalization and approximation components, with the latter given by  $\inf_{f \in \mathcal{F}} R(f)$ . While this quantity is not directly observable, it is monotone

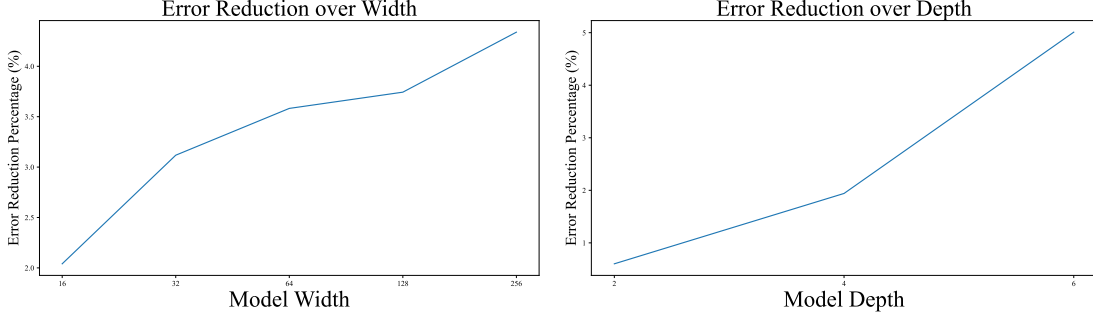


Fig. 2. Reconstruction error reduction in percentage with MCR. **Left:** The error reduction percentage over varying model width. **Right:** The error reduction percentage over varying model depth.

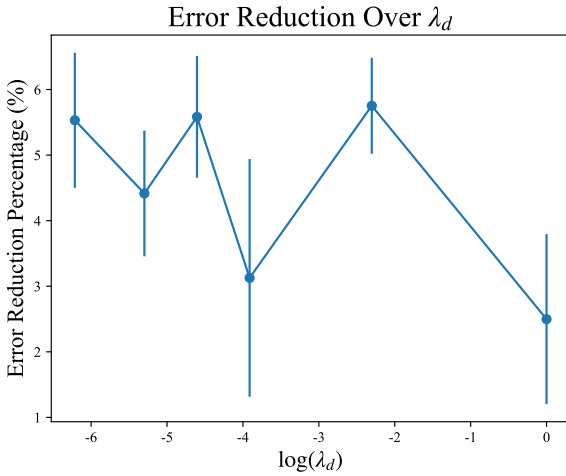


Fig. 3. Error reduction vs  $\log \lambda_d$ . We do not observe a statistically significant trend across different  $\lambda_d$ .

with respect to model class inclusion: if  $\mathcal{F}_1 \subseteq \mathcal{F}_2$ , then  $\inf_{f \in \mathcal{F}_1} R(f) \geq \inf_{f \in \mathcal{F}_2} R(f)$ . Moreover, Theorem 1 predicts that as approximation error decreases, the relative contribution of the estimation error reduction induced by MCR becomes dominant.

We examine this effect by systematically increasing model capacity, varying both the width (from 16 to 256 hidden units) and depth (from 2 to 6 layers) of the MLP predictor, while keeping  $n$  and  $m$  fixed. Figure 2 shows that the reconstruction error reduction percentage increases monotonically with both width and depth. Since the generalization bounds remain unchanged across these settings, the observed trend directly reflects decreasing approximation error, confirming that MCR becomes increasingly advantageous for richer function classes.

*Effect of the MCR weight  $\lambda_d$ .*: Our theoretical guarantees are conditioned on achieving a nonzero but finite training loss tolerance  $\epsilon_{\mathcal{L}}$ , and do not depend explicitly on the choice of  $\lambda_d$ . Consequently, we expect comparable performance gains across a broad range of  $\lambda_d$  values, provided that training reaches the prescribed loss threshold.

To verify this, we fix  $(n, m)$  at the best-performing configuration from Table II and use a two-layer MLP with width 64. We vary  $\lambda_d \in \{0.002, 0.005, 0.01, 0.02, 0.1, 1\}$ ,

training each model until  $\epsilon_{\mathcal{L}} \leq 0.003$  and the duality gap stopping condition is satisfied. As shown in Fig. 3, there is no statistically significant trend across different  $\lambda_d$  values, confirming that  $\lambda_d$  primarily affects optimization dynamics rather than the theoretical benefit of MCR. In practice, we therefore recommend choosing  $\lambda_d$  small enough to avoid impeding convergence of the primary loss  $\mathcal{L}$ .

*Choice of neural net distance  $\mathcal{G}_{nn}$ .*: While our imperfect-training analysis relies on loss dominance conditions, the underlying intuition of MCR, constraining the imputed distribution to remain close to the fully observed one, should hold across a range of discrepancy measures. To assess this robustness, we compare MCR using Gaussian-kernel MMD (bandwidth 1) and 1-Wasserstein distance.

We vary the ratio  $m/n \in \{2, 10, 20\}$  and the model width in  $\{64, 128, 256\}$ , while fixing depth at 4 and  $n = 100$ . The results, reported in Table III, show that Wasserstein-based MCR typically achieves slightly larger error reductions, though MMD-based MCR also yields consistent and statistically significant improvements in most settings. This aligns with the fact that MMD can be  $(C, \alpha)$ -dominated by RMSE under suitable RKHS smoothness assumptions. Nonetheless, we recommend selecting the neural net distance in accordance with the consistency considerations summarized in Table I.

*Increasing distribution discrepancy  $\xi$ .*: We next examine the effect of the distribution discrepancy  $\xi$ . According to our theory, the benefit of MCR disappears once the viability condition in Eq. (13) is satisfied, beyond which MCR may negatively impact generalization. To empirically verify this behavior, we construct a controlled experiment in which  $\xi$  is increased while all other factors are fixed.

Specifically, we inject an artificial mean shift into the sampled data, with shift magnitudes in

$$[0.0, 0.25, 0.5, 0.75, 1.0, 1.5, 2.0, 3.0, 4.0],$$

thereby inducing increasing distribution discrepancy. The data ratio and model architecture are fixed at their empirically optimal settings, and 5 Monte Carlo runs are performed for each shift level. Since true  $\xi$  is intractable in practice, we resolve to the calibrated discrepancy estimation  $\hat{\xi}$  in (12). As shown in Fig. 4, the error reduction steadily declines as  $\hat{\xi}$  increases. Plotting error reduction against  $\hat{\xi}$  shows that the threshold implied by Eq. (13) lies near the no-improvement

TABLE III

RECONSTRUCTION ERROR REDUCTION PERCENTAGE (%) WITH MCR. ON COLUMNS TITLE, WE HAVE THE  $m/n$  RATIO. ON ROWS TITLE, WE HAVE THE MODEL WIDTHS. IN EACH CELL, WE SHOW MMD PERFORMANCE ON THE LEFT, AND 1-WASSERSTEIN DISTANCE PERFORMANCE ON THE RIGHT. THE HIGHER VALUE IN EACH CELL IS MARKED IN **BOLD**.

$m/n$	Model Width	64	128	256
2		<b><math>2.05 \pm 0.54</math></b> / $1.86 \pm 0.61$	$2.66 \pm 0.54$ / <b><math>2.98 \pm 0.36</math></b>	$2.84 \pm 0.60$ / <b><math>3.08 \pm 0.54</math></b>
10		$0.24 \pm 0.41$ / <b><math>0.76 \pm 0.44</math></b>	$3.40 \pm 0.50$ / <b><math>3.69 \pm 1.11</math></b>	$3.14 \pm 0.37$ / <b><math>3.42 \pm 0.46</math></b>
20		$0.79 \pm 0.77$ / <b><math>1.71 \pm 0.98</math></b>	$2.99 \pm 0.44$ / <b><math>3.81 \pm 0.18</math></b>	$4.15 \pm 0.35$ / <b><math>4.98 \pm 0.82</math></b>

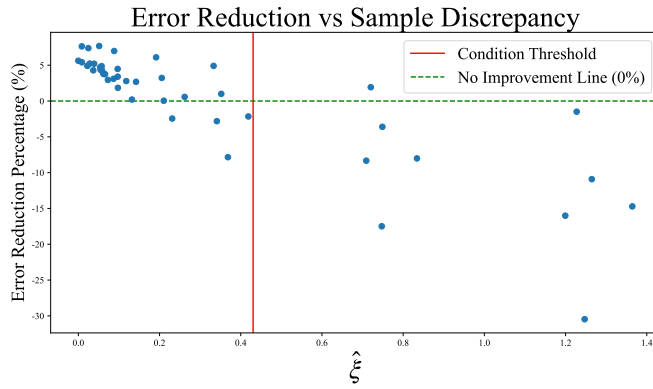


Fig. 4. Error reduction vs  $\hat{\xi}$ . The condition threshold in Eq. (13) based on our  $\hat{\xi}$  estimates in Eq. (12) accurately reflects the tipping point where MCR’s benefit disappears.

results, with MCR beginning to degrade test performance once  $\hat{\xi}$  exceeds this condition.

### B. Evaluating the Duality Gap Stopping Condition

We now examine the effectiveness of the duality gap stopping condition. Importantly, this criterion does not alter the MCR training process itself; rather, it determines the appropriate stopping point in Algorithm 1. Experimental settings are detailed in the supplementary materials. Using the same synthetic data and model configuration as in Sec. VI-A, we train both vanilla and MCR models for 2000 epochs. To ensure comparability, we apply the same optimizer and learning rate across both settings. Convergence of  $\theta$  in Algorithm 1 is defined by the training loss  $\mathcal{L}$  (not the neural net distance) stabilizing within 0.00005 over five consecutive epochs.

Figure 5 reports the test error comparisons alongside the stopping points selected by the duality gap condition. On the left, we show the full 2000-epoch curves, overlaying two key markers: (i) the average duality gap stopping epoch (770), and (ii) the performance divergence epoch (830), defined as the first point where the test error confidence intervals of vanilla and MCR training no longer overlap. The right panel zooms in on the first 100 epochs. Several observations emerge:

- 1) MCR training achieves consistently lower test error compared with vanilla training, confirming its robustness advantage.
- 2) The average duality gap stopping epoch is close to the performance divergence epoch, demonstrating that the duality gap condition serves as a reliable early indicator of generalization gains, in line with Corollary 4.

- 3) In the initial training phase, MCR temporarily yields higher test error compared with vanilla training. This phenomenon reflects the theoretical insight from Theorem 2 that performance gains are not guaranteed at all stages, and it empirically confirms the existence of “bad” MCR training phases.

### C. Versatility of MCR

As discussed in earlier sections, measure consistency regularization (MCR) has already been adopted across a range of machine learning tasks, reflecting its flexibility and broad applicability. Building on the theoretical foundations and synthetic simulations presented previously, the purpose of this subsection is to provide concrete examples of how MCR improves performance in real-world settings. By doing so, we aim to highlight the versatility of MCR when paired with diverse model architectures and data modalities. In each case, we measure reconstruction error using RMSE between the imputed output and the ground-truth target. We train with MCR extensively to make sure the duality gap stopping condition is satisfied.

#### Image Reconstruction:

We begin with image data, where the task is to reconstruct missing image regions. Specifically, we crop out the lower half of images in MNIST and CIFAR10 and use the upper half to impute the missing pixels. Prediction functions are implemented using a convolutional encoder-decoder architecture.

The quantitative results, shown in Fig. 7 (left), demonstrate that models trained with MCR consistently achieve smaller reconstruction error. A qualitative comparison for MNIST reconstructions is provided in Fig. 6, where MCR training produces visually more plausible digits. Overall, these experiments show that MCR improves structured image reconstruction both quantitatively and qualitatively.

#### Sensor Data Imputation:

We next consider sensor fusion tasks, which highlight the use of MCR for cross-modal imputation. Here, ECG signals are imputed using TEB and EDA data from the Activity dataset [63], and optical sensor data are imputed from radar measurements in the Crop dataset [64], [65]. For both tasks, we employ variational autoencoders as the prediction function class.

As shown in Fig. 7 (center), MCR-trained models consistently outperform baselines. This indicates that the MCR not only improves within-modality tasks, such as image reconstruction, but also provides measurable benefits in more challenging cross-modal settings.

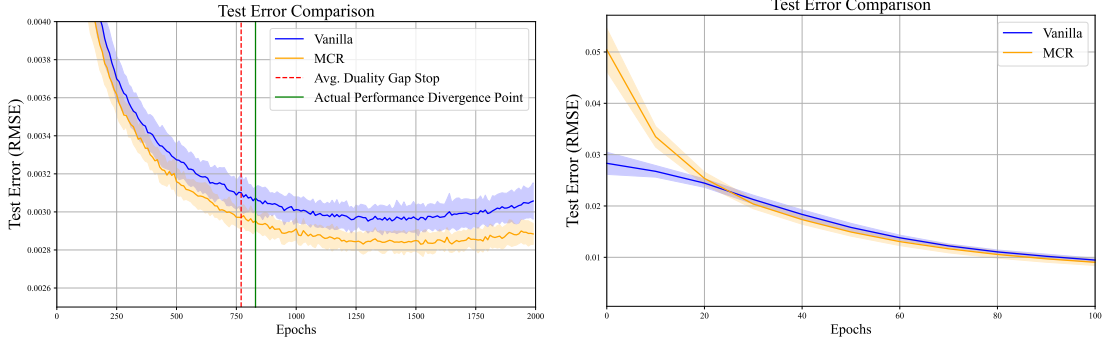


Fig. 5. The test error curve comparison between vanilla training and MCR training. **Left:** Test error curve over 2000 epochs. **Right:** Test error curve comparison in the first 100 epochs.



Fig. 6. Reconstruction comparison on MNIST dataset. The first row shows the input half-images for reconstruction. The second row shows the reconstruction results for the model trained without MCR, and the third row shows the results for model trained with MCR.

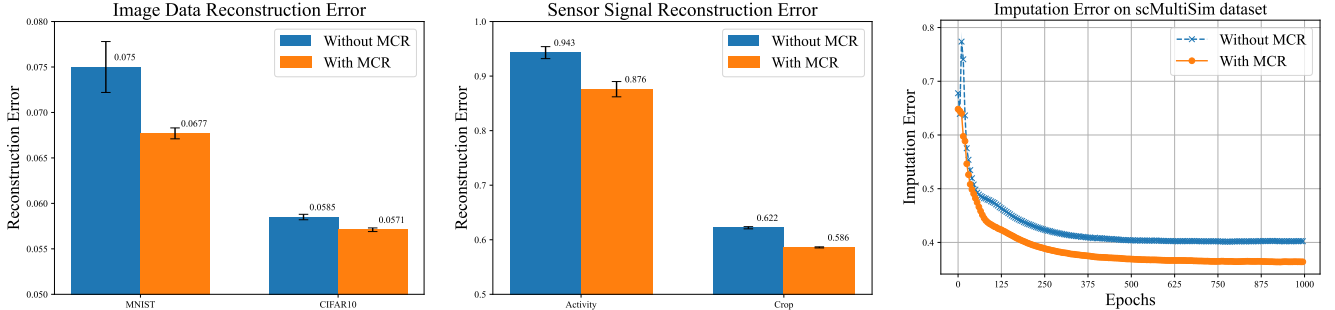


Fig. 7. **Left:** Image reconstruction error comparison. **Center:** Sensor data imputation error comparison. Models trained with MCR achieve consistently lower error compared to one without MCR. **Right:** ATAC-Seq imputation error comparison for MultiVI model trained with and without MCR. Note that specifically for ATAC-Seq imputation, the training loss for both cases (with and without MCR) behave similarly, converging to  $0.0043 \pm 0.00015$  vs.  $0.0041 \pm 0.00006$ . The loss curve for epochs are averaged over 20 runs.

### Single-Cell Data Integration:

Finally, we evaluate MCR in the context of single-cell multiomic data integration. As profiling a single cell typically yields only one modality, imputing complementary modalities has become a critical challenge in single-cell analysis [66]. We focus on imputing ATAC-seq data from RNA counts using the state-of-the-art MultiVI model [13]. MultiVI employs two variational autoencoders coupled through a shared latent space: during training, the latent prior is the average of both modalities, while at inference it relies only on RNA embeddings. We use the scMultiSim dataset [67] for evaluation.

The results in Fig. 7 (right) show that MCR-trained MultiVI consistently achieves lower imputation error. We note that

both MCR-trained and vanilla MultiVI achieve similar training loss values at epoch 1000 ( $0.0043 \pm 0.00015$  vs.  $0.0041 \pm 0.00006$ ), the MCR-trained models yield better generalization performance.

Taken together, these real-world experiments complement our theoretical analysis by illustrating the robustness and versatility of MCR across diverse domains: structured vision tasks, cross-modal sensor data, and high-dimensional biological data.

## VII. CONCLUSION

In this work, we have presented a unified framework for measure consistency regularization (MCR) in imputation tasks involving partially observed datasets. Our analysis focused

on the theoretical underpinnings of MCR through the lens of neural net distance, leading to estimation error bounds that address both the perfect and imperfect training regimes. This analysis provides answers to three critical questions concerning the benefits of MCR. Under perfect training, we showed that the primary advantage arises from a reduction in the estimation error upper bound. In the imperfect training regime, we established that robustness is guaranteed only under a specific analytical condition. Building on this insight, we proposed a duality gap based training protocol that ensures, with high probability, the robustness benefits of MCR.

We validated these theoretical findings through extensive simulations, examining different aspects of the error bounds and the proposed training protocol. Furthermore, we demonstrated the versatility of MCR across a range of real-world datasets, spanning structured image reconstruction, cross-modal sensor data imputation, and single-cell data integration. Together, these results highlight both the theoretical soundness and the practical utility of MCR.

Beyond imputation, we believe our work has broader implications. The imputation framework considered here is closely related to post-training methods widely adopted in large language models (LLMs). As such, our theoretical analysis could be extended to two-stage training frameworks, offering new insights into the mechanisms and effectiveness of post-training in modern machine learning systems.

#### ACKNOWLEDGMENT

This work was initiated when Yinsong Wang was at Northeastern University and the work is supported by the NSF Award #2038625 as part of the NSF/DHS/DOT/NIH/USDA-NIFA Cyber-Physical Systems Program.

#### REFERENCES

- [1] E. Swanson, C. Lord, J. Reading, A. T. Heubeck, P. C. Genge, Z. Thomson, M. D. Weiss, X.-j. Li, A. K. Savage, R. R. Green, T. R. Torgerson, T. F. Bumol, L. T. Graybuck, and P. J. Skene, “Simultaneous trimodal single-cell measurement of transcripts, epitopes, and chromatin accessibility using TEA-seq,” *Elife*, vol. 10, p. e63632, 2021.
- [2] E. P. Mimitou, C. A. Lareau, K. Y. Chen, A. L. Zorzetto-Fernandes, Y. Hao, Y. Takeshima, W. Luo, T.-S. Huang, B. Z. Yeung, E. Papalexis, P. I. Thakore, T. Kibayashi, J. B. Wing, M. Hata, R. Satija, K. I. Nazor, S. Sakaguchi, L. S. Ludwig, V. G. Sankaran, A. Regev, and P. Smibert, “Scalable, multimodal profiling of chromatin accessibility, gene expression and protein levels in single cells,” *Nature Biotechnology*, vol. 39, no. 10, pp. 1246–1258, 2021.
- [3] A. Choudhury, “Missing data imputation using machine learning and natural language processing for clinical diagnostic codes,” Ph.D. dissertation, The University of North Carolina at Chapel Hill, 2020.
- [4] P. J. García-Laencina, J.-L. Sancho-Gómez, A. R. Figueiras-Vidal, and M. Verleysen, “K nearest neighbours with mutual information for simultaneous classification and missing data imputation,” *Neurocomputing*, vol. 72, no. 7-9, pp. 1483–1493, 2009.
- [5] L. Yu, L. Liu, and K. E. Peace, “Regression multiple imputation for missing data analysis,” *Statistical Methods in Medical Research*, vol. 29, no. 9, pp. 2647–2664, 2020.
- [6] Y. Zhao and Q. Long, “Multiple imputation in the presence of high-dimensional data,” *Statistical Methods in Medical Research*, vol. 25, no. 5, pp. 2021–2035, 2016.
- [7] L. Tran, X. Liu, J. Zhou, and R. Jin, “Missing modalities imputation via cascaded residual autoencoder,” in *Proceedings of the IEEE conference on computer vision and pattern recognition*, 2017, pp. 1405–1414.
- [8] M. Ma, J. Ren, L. Zhao, S. Tulyakov, C. Wu, and X. Peng, “Smil: Multimodal learning with severely missing modality,” in *Proceedings of the AAAI Conference on Artificial Intelligence*, vol. 35, no. 3, 2021, pp. 2302–2310.
- [9] T. Joy, Y. Shi, P. Torr, T. Rainforth, S. M. Schmon, and N. Siddharth, “Learning multimodal vaes through mutual supervision,” in *International Conference on Learning Representations*, 2021.
- [10] J. Sun, X. Zhang, S. Han, Y.-P. Ruan, and T. Li, “Redcore: Relative advantage aware cross-modal representation learning for missing modalities with imbalanced missing rates,” in *Proceedings of the AAAI Conference on Artificial Intelligence*, vol. 38, no. 13, 2024, pp. 15 173–15 182.
- [11] M. Kang, R. Zhu, D. Chen, X. Liu, and W. Yu, “Cm-gan: A cross-modal generative adversarial network for imputing completely missing data in digital industry,” *IEEE Transactions on Neural Networks and Learning Systems*, 2023.
- [12] C. Cheng, G. Cheng, and J. C. Duchi, “Collaboratively learning linear models with structured missing data,” *Advances in Neural Information Processing Systems*, vol. 36, 2024.
- [13] T. Ashuach, M. I. Gabitto, R. V. Koodli, G.-A. Saldi, M. I. Jordan, and N. Yosef, “Multivi: deep generative model for the integration of multimodal data,” *Nature Methods*, vol. 20, no. 8, pp. 1222–1231, 2023.
- [14] X. Tu, Z.-J. Cao, S. Mostafavi, G. Gao *et al.*, “Cross-linked unified embedding for cross-modality representation learning,” *Advances in Neural Information Processing Systems*, vol. 35, pp. 15 942–15 955, 2022.
- [15] B. Gong, Y. Zhou, and E. Purdom, “Cobolt: integrative analysis of multimodal single-cell sequencing data,” *Genome biology*, vol. 22, pp. 1–21, 2021.
- [16] O. Elharrouss, N. Almaadeed, S. Al-Maadeed, and Y. Akbari, “Image inpainting: A review,” *Neural Processing Letters*, vol. 51, no. 2, pp. 2007–2028, 2020.
- [17] N. Cohen Kalafut, X. Huang, and D. Wang, “Joint variational autoencoders for multimodal imputation and embedding,” *Nature Machine Intelligence*, vol. 5, no. 6, pp. 631–642, 2023.
- [18] R. Mitra, S. F. McGough, T. Chakraborti, C. Holmes, R. Copping, N. Hagenbuch, S. Biedermann, J. Noonan, B. Lehmann, A. Shenvi *et al.*, “Learning from data with structured missingness,” *Nature Machine Intelligence*, vol. 5, no. 1, pp. 13–23, 2023.
- [19] N. Bahador, J. Jokelainen, S. Mustola, and J. Kortelainen, “Reconstruction of missing channel in electroencephalogram using spatiotemporal correlation-based averaging,” *Journal of Neural Engineering*, vol. 18, no. 5, p. 056045, 2021.
- [20] W. Hou, Z. Ji, H. Ji, and S. C. Hicks, “A systematic evaluation of single-cell rna-sequencing imputation methods,” *Genome biology*, vol. 21, pp. 1–30, 2020.
- [21] S. Yoon and S. Sull, “Gamin: Generative adversarial multiple imputation network for highly missing data,” in *Proceedings of the IEEE/CVF conference on computer vision and pattern recognition*, 2020, pp. 8456–8464.
- [22] J. Yoon, J. Jordon, and M. Schaar, “Gain: Missing data imputation using generative adversarial nets,” in *International conference on machine learning*. PMLR, 2018, pp. 5689–5698.
- [23] B. Muzellec, J. Josse, C. Boyer, and M. Cuturi, “Missing data imputation using optimal transport,” in *International Conference on Machine Learning*. PMLR, 2020, pp. 7130–7140.
- [24] Y. Wu, X. Miao, X. Huang, and J. Yin, “Jointly imputing multi-view data with optimal transport,” in *Proceedings of the AAAI Conference on Artificial Intelligence*, vol. 37, no. 4, 2023, pp. 4747–4755.
- [25] S. Arora, R. Ge, Y. Liang, T. Ma, and Y. Zhang, “Generalization and equilibrium in generative adversarial nets (GANs),” in *Proceedings of the 34th International Conference on Machine Learning*, ser. Proceedings of Machine Learning Research, D. Precup and Y. W. Teh, Eds., vol. 70. PMLR, 06–11 Aug 2017, pp. 224–232. [Online]. Available: <https://proceedings.mlr.press/v70/arora17a.html>
- [26] F. Taherkhani, A. Dabouei, S. Soleymani, J. Dawson, and N. M. Nasrabadi, “Self-supervised wasserstein pseudo-labeling for semi-supervised image classification,” in *Proceedings of the IEEE/CVF conference on computer vision and pattern recognition*, 2021, pp. 12 267–12 277.
- [27] M. Śmieja, Ł. Struski, J. Tabor, B. Zieliński, and P. Spurek, “Processing of missing data by neural networks,” *The 2018 Advances in Neural Information Processing Systems*, vol. 31, Dec 2018.
- [28] A. Farahani, S. Vogheli, K. Rasheed, and H. R. Arabnia, “A brief review of domain adaptation,” *Advances in Data Science and Information Engineering: Proceedings from ICDATA 2020 and IKE 2020*, pp. 877–894, 2021.
- [29] J. E. Van Engelen and H. H. Hoos, “A survey on semi-supervised learning,” *Machine Learning*, vol. 109, no. 2, pp. 373–440, 2020.
- [30] D. Berthelot, N. Carlini, I. Goodfellow, N. Papernot, A. Oliver, and C. A. Raffel, “Mixmatch: A holistic approach to semi-supervised learning,” *Advances in neural information processing systems*, vol. 32, 2019.

[31] K. Sohn, D. Berthelot, N. Carlini, Z. Zhang, H. Zhang, C. A. Raffel, E. D. Cubuk, A. Kurakin, and C.-L. Li, “Fixmatch: Simplifying semi-supervised learning with consistency and confidence,” *Advances in neural information processing systems*, vol. 33, pp. 596–608, 2020.

[32] Z. Huang, L. Shen, J. Yu, B. Han, and T. Liu, “Flatmatch: Bridging labeled data and unlabeled data with cross-sharpness for semi-supervised learning,” *Advances in Neural Information Processing Systems*, vol. 36, 2024.

[33] Q. Wang, W. Li, and L. V. Gool, “Semi-supervised learning by augmented distribution alignment,” in *Proceedings of the IEEE/CVF international conference on computer vision*, 2019, pp. 1466–1475.

[34] R. Fortet and E. Mourier, “Convergence de la répartition empirique vers la répartition théorique,” *Annales scientifiques de l’École Normale Supérieure*, vol. 3e série, 70, no. 3, pp. 267–285, 1953. [Online]. Available: <http://www.numdam.org/articles/10.24033/asens.1013/>

[35] L. V. Kantorovich and S. Rubinshtein, “On a space of totally additive functions,” *Vestnik of the St. Petersburg University: Mathematics*, vol. 13, no. 7, pp. 52–59, 1958.

[36] S. T. Rachev, L. B. Klebanov, S. V. Stoyanov, and F. Fabozzi, *The methods of distances in the theory of probability and statistics*. Springer, 2013, vol. 10.

[37] C. Villani *et al.*, *Optimal Transport: Old and New*. Springer, 2008, vol. 338.

[38] M. Arjovsky, S. Chintala, and L. Bottou, “Wasserstein generative adversarial networks,” in *International conference on machine learning*. PMLR, 2017, pp. 214–223.

[39] H. Zhao, K. Sun, A. Dezfooli, and E. V. Bonilla, “Transformed distribution matching for missing value imputation,” in *International Conference on Machine Learning*. PMLR, 2023, pp. 42159–42186.

[40] P. Zhang, Q. Liu, D. Zhou, T. Xu, and X. He, “On the discrimination-generalization tradeoff in gans,” *arXiv preprint arXiv:1711.02771*, 2017.

[41] I. Gulrajani, F. Ahmed, M. Arjovsky, V. Dumoulin, and A. C. Courville, “Improved training of wasserstein gans,” *Advances in neural information processing systems*, vol. 30, 2017.

[42] F. Taherkhani, A. Dabouei, S. Soleymani, J. Dawson, and N. M. Nasrabadi, “Transporting labels via hierarchical optimal transport for semi-supervised learning,” in *Computer Vision–ECCV 2020: 16th European Conference, Glasgow, UK, August 23–28, 2020, Proceedings, Part IV 16*. Springer, 2020, pp. 509–526.

[43] K. Ji and Y. Liang, “Minimax estimation of neural net distance,” *Advances in Neural Information Processing Systems*, vol. 31, 2018.

[44] K. Ji, Y. Zhou, and Y. Liang, “Understanding estimation and generalization error of generative adversarial networks,” *IEEE Transactions on Information Theory*, vol. 67, no. 5, pp. 3114–3129, 2021.

[45] T. Liang, “How well can generative adversarial networks learn densities: A nonparametric view,” *arXiv preprint arXiv:1712.08244*, 2017.

[46] M. Long, Z. Cao, J. Wang, and M. I. Jordan, “Conditional adversarial domain adaptation,” *Advances in neural information processing systems*, vol. 31, 2018.

[47] J. Li, E. Chen, Z. Ding, L. Zhu, K. Lu, and H. T. Shen, “Maximum density divergence for domain adaptation,” *IEEE transactions on pattern analysis and machine intelligence*, vol. 43, no. 11, pp. 3918–3930, 2020.

[48] L. Heumos, A. C. Schaar, C. Lance, A. Litinetskaya, F. Drost, L. Zappia, M. D. Lücken, D. C. Strobl, J. Henao, F. Curioni *et al.*, “Best practices for single-cell analysis across modalities,” *Nature Reviews Genetics*, vol. 24, no. 8, pp. 550–572, 2023.

[49] A. Gayoso, Z. Steier, R. Lopez, J. Regier, K. L. Nazor, A. Streets, and N. Yosef, “Joint probabilistic modeling of single-cell multi-omic data with totalvi,” *Nature methods*, vol. 18, no. 3, pp. 272–282, 2021.

[50] C. Zhang, L. Zhang, and J. Ye, “Generalization bounds for domain adaptation,” *Advances in neural information processing systems*, vol. 25, 2012.

[51] M. Fazlyab, A. Robey, H. Hassani, M. Morari, and G. Pappas, “Efficient and accurate estimation of lipschitz constants for deep neural networks,” *Advances in neural information processing systems*, vol. 32, 2019.

[52] T. Akidau, R. Bradshaw, C. Chambers, S. Chernyak, R. J. Fernández-Moctezuma, R. Lax, S. McVeety, D. Mills, F. Perry, E. Schmidt *et al.*, “The dataflow model: a practical approach to balancing correctness, latency, and cost in massive-scale, unbounded, out-of-order data processing,” *Proceedings of the VLDB Endowment*, vol. 8, no. 12, pp. 1792–1803, 2015.

[53] J. Cheng, Q. Li, T. Lin, and Z. Shen, “Interpolation, approximation, and controllability of deep neural networks,” *SIAM Journal on Control and Optimization*, vol. 63, no. 1, pp. 625–649, 2025.

[54] S. Ben-David, T. Lu, and D. Pál, “Does unlabeled data provably help? worst-case analysis of the sample complexity of semi-supervised learning,” in *COLT*, 2008, pp. 33–44.

[55] A. Singh, R. Nowak, and J. Zhu, “Unlabeled data: Now it helps, now it doesn’t,” *Advances in neural information processing systems*, vol. 21, 2008.

[56] P. L. Bartlett, D. J. Foster, and M. J. Telgarsky, “Spectrally-normalized margin bounds for neural networks,” *Advances in neural information processing systems*, vol. 30, 2017.

[57] A. L. Gibbs and F. E. Su, “On choosing and bounding probability metrics,” *International Statistical Review*, vol. 70, no. 3, pp. 419–435, 2002.

[58] D. Prandi, “Hölder equivalence of the value function for control-affine systems,” *ESAIM: Control, Optimisation and Calculus of Variations*, vol. 20, no. 4, pp. 1224–1248, 2014.

[59] J. Mitchell, “On carnot-caratheodory metrics,” *Journal of Differential Geometry*, vol. 21, no. 1, pp. 35–45, 1985.

[60] P. Grnarova, K. Y. Levy, A. Lucchi, N. Perraudeau, I. Goodfellow, T. Hofmann, and A. Krause, “A domain agnostic measure for monitoring and evaluating gans,” *Advances in neural information processing systems*, vol. 32, 2019.

[61] S. Sidhekh, A. Aimen, V. Madan, and N. C. Krishnan, “On duality gap as a measure for monitoring gan training,” in *2021 international joint conference on neural networks (IJCNN)*. IEEE, 2021, pp. 1–8.

[62] S. Sidhekh, A. Aimen, and N. C. Krishnan, “On characterizing gan convergence through proximal duality gap,” in *International Conference on Machine Learning*. PMLR, 2021, pp. 9660–9670.

[63] I. Mohino-Herranz, R. Gil-Pita, M. Rosa-Zurera, and F. Seoane, “Activity recognition using wearable physiological measurements: Selection of features from a comprehensive literature study,” *Sensors*, vol. 19, no. 24, 2019.

[64] I. Khosravi, A. Safari, and S. Homayouni, “Msmd: maximum separability and minimum dependency feature selection for cropland classification from optical and radar data,” *International Journal of Remote Sensing*, vol. 39, no. 8, pp. 2159–2176, 2018.

[65] I. Khosravi and S. K. Alavipanah, “A random forest-based framework for crop mapping using temporal, spectral, textural and polarimetric observations,” *International Journal of Remote Sensing*, vol. 40, no. 18, pp. 7221–7251, 2019.

[66] G. C. Linderman, J. Zhao, M. Roulis, P. Bielecki, R. A. Flavell, B. Nadler, and Y. Kluger, “Zero-preserving imputation of single-cell RNA-seq data,” *Nature communications*, vol. 13, no. 1, p. 192, 2022.

[67] H. Li, Z. Zhang, M. Squires, X. Chen, and X. Zhang, “scmultisim: simulation of multi-modality single cell data guided by cell-cell interactions and gene regulatory networks,” *Research Square*, 2022.

[68] M. Mohri, A. Rostamizadeh, and A. Talwalkar, *Foundations of Machine Learning*. MIT press, 2018.



Yinsong Wang

Yinsong Wang received his B.S. degree in Mechanical Engineering from Shandong University, China, in 2017, his M.S. degree in Manufacturing System Engineering and Management from The Hong Kong Polytechnic University, Hong Kong, in 2018, and his Ph.D. degree in Industrial Engineering at Northeastern University, USA, in 2024. He is currently a Postdoctoral Fellow in the H. Milton Stewart School of Industrial & Systems Engineering at Georgia Institute of Technology. His research interests include machine learning, data science, and

kernel methods.



Shahin Shahrampour received the Ph.D. degree in Electrical and Systems Engineering, the M.A. degree in Statistics (The Wharton School), and the M.S.E. degree in Electrical Engineering, all from the University of Pennsylvania, in 2015, 2014, and 2012, respectively. He is currently an Assistant Professor in the Department of Mechanical and Industrial Engineering at Northeastern University. His research interests include machine learning, optimization, sequential decision-making, and distributed learning, with a focus on developing computationally efficient

methods for data analytics. He is a Senior Member of the IEEE.

## APPENDIX

## Omitted Proofs

*Proof of Theorem 1:* We decompose the estimation error for a prediction function  $\hat{f}$  into the following three parts

$$\begin{aligned}
& d_{\mathcal{G}_{nn}}(\boldsymbol{\pi}, \boldsymbol{\pi}^{\hat{f}}) - \inf_{f \in \mathcal{F}} d_{\mathcal{G}_{nn}}(\boldsymbol{\pi}, \boldsymbol{\pi}^f) \\
&= \underbrace{d_{\mathcal{G}_{nn}}(\boldsymbol{\pi}, \boldsymbol{\pi}^{\hat{f}}) - d_{\mathcal{G}_{nn}}(\boldsymbol{\pi}_l, \boldsymbol{\pi}^{\hat{f}})}_{\textcircled{1}} \\
&\quad + \underbrace{d_{\mathcal{G}_{nn}}(\boldsymbol{\pi}_l, \boldsymbol{\pi}^{\hat{f}}) - \inf_{f \in \mathcal{F}} d_{\mathcal{G}_{nn}}(\boldsymbol{\pi}_l, \boldsymbol{\pi}^f)}_{\textcircled{2}} \\
&\quad + \underbrace{\inf_{f \in \mathcal{F}} d_{\mathcal{G}_{nn}}(\boldsymbol{\pi}_l, \boldsymbol{\pi}^f) - \inf_{f \in \mathcal{F}} d_{\mathcal{G}_{nn}}(\boldsymbol{\pi}, \boldsymbol{\pi}^f)}_{\textcircled{3}}.
\end{aligned} \tag{15}$$

We now need Lemma 5 to proceed with our bound.

**Lemma 5.** [68] For functions  $h \in \mathcal{H}$  with maximum output size  $B_h$ , denoting the true measure as  $\boldsymbol{\pi}$  and empirical measure of  $n$  data points as  $\boldsymbol{\pi}_l$ , we can bound the following quantity with probability at least  $1 - \delta$

$$\sup_{h \in \mathcal{H}} [\boldsymbol{\pi}h - \boldsymbol{\pi}_l h] \leq 2\hat{\mathfrak{R}}_n(\mathcal{H}) + \frac{3B_h\sqrt{\ln \delta^{-1}}}{\sqrt{2n}},$$

where  $\hat{\mathfrak{R}}_n(\mathcal{H})$  is the Rademacher complexity of function class  $\mathcal{H}$  over  $n$  data points, defined as

$$\hat{\mathfrak{R}}_n(\mathcal{H}) := \mathbb{E}_\sigma \left[ \sup_{h \in \mathcal{H}} \frac{1}{n} \sum_{i=1}^n \sigma_i h(\mathbf{x}_i) \right], \tag{16}$$

where  $\{\sigma_i\}_{i=1}^n$  are i.i.d. random variables uniformly sampled from  $\{\pm 1\}$ .

Term  $\textcircled{1}$  is easy to bound by rewriting the formulation for any prediction  $f \in \mathcal{F}$  as follows

$$\begin{aligned}
& d_{\mathcal{G}_{nn}}(\boldsymbol{\pi}, \boldsymbol{\pi}^f) - d_{\mathcal{G}_{nn}}(\boldsymbol{\pi}_l, \boldsymbol{\pi}^f) \\
&= \sup_{g \in \mathcal{G}_{nn}} [\boldsymbol{\pi}g - \boldsymbol{\pi}^f g] - \sup_{g \in \mathcal{G}_{nn}} [\boldsymbol{\pi}_l g - \boldsymbol{\pi}^f g] \\
&\leq \sup_{g \in \mathcal{G}_{nn}} [\boldsymbol{\pi}g - \boldsymbol{\pi}_l g].
\end{aligned} \tag{17}$$

Note that we rely on the symmetry of  $\mathcal{G}_{nn}$  to switch between  $\sup_{g \in \mathcal{G}_{nn}} [\boldsymbol{\pi}g - \boldsymbol{\pi}^f g]$  and  $\sup_{g \in \mathcal{G}_{nn}} |\boldsymbol{\pi}g - \boldsymbol{\pi}^f g|$ . Let  $f' = \arg\min\{d_{\mathcal{G}_{nn}}(\boldsymbol{\pi}, \boldsymbol{\pi}^f)\}$ . Then, for Term  $\textcircled{3}$ , we have

$$\begin{aligned}
& \inf_{f \in \mathcal{F}} d_{\mathcal{G}_{nn}}(\boldsymbol{\pi}_l, \boldsymbol{\pi}^f) - \inf_{f \in \mathcal{F}} d_{\mathcal{G}_{nn}}(\boldsymbol{\pi}, \boldsymbol{\pi}^f) \\
&\leq d_{\mathcal{G}_{nn}}(\boldsymbol{\pi}_l, \boldsymbol{\pi}^{f'}) - d_{\mathcal{G}_{nn}}(\boldsymbol{\pi}, \boldsymbol{\pi}^{f'}) \\
&= \sup_{g \in \mathcal{G}_{nn}} [\boldsymbol{\pi}_l g - \boldsymbol{\pi}^{f'} g] - \sup_{g \in \mathcal{G}_{nn}} [\boldsymbol{\pi}g - \boldsymbol{\pi}^{f'} g] \\
&\leq \sup_{g \in \mathcal{G}_{nn}} [\boldsymbol{\pi}_l g - \boldsymbol{\pi}g] = \sup_{g \in \mathcal{G}_{nn}} [\boldsymbol{\pi}g - \boldsymbol{\pi}_l g],
\end{aligned}$$

where the last line holds for any symmetric  $\mathcal{G}_{nn}$  (i.e.,  $g \in \mathcal{G}_{nn} \Rightarrow -g \in \mathcal{G}_{nn}$ ). Notice that the above bound is independent

of  $f$  and is only dependent on the fully observed dataset  $\mathbf{D}_l$  and  $\mathcal{G}_{nn}$ .

We next bound the upper bound term in (17). With Lemma 5, we have the upper bound with probability at least  $1 - \delta$  such that

$$\sup_{g \in \mathcal{G}_{nn}} [\boldsymbol{\pi}g - \boldsymbol{\pi}_l g] \leq 2\hat{\mathfrak{R}}_n(\mathcal{G}_{nn}) + \frac{3B_g B_{xz} \sqrt{\ln \delta^{-1}}}{\sqrt{2n}},$$

and therefore, we conclude that

$$\textcircled{1} + \textcircled{3} \leq 4\hat{\mathfrak{R}}_n(\mathcal{G}_{nn}) + \frac{3B_g B_{xz} \sqrt{2 \ln \delta^{-1}}}{\sqrt{n}}. \tag{18}$$

The major difference between the prediction function learned with and without MCR comes down to the difference in Term  $\textcircled{2}$ .

We denote by  $f_l^*$  the prediction function learned without MCR on  $\mathbf{D}_l$ , and by  $f_u^*$  the prediction function learned with MCR using both  $\mathbf{D}_l$  and  $\mathbf{D}_u$ . Assume that the best prediction function in terms of the neural distance under  $\mathcal{G}_{nn}$  is  $\tilde{f}$ . Then, for  $f_l^*$ , we have the following

$$\begin{aligned}
& d_{\mathcal{G}_{nn}}(\boldsymbol{\pi}_l, \boldsymbol{\pi}^{f_l^*}) - \inf_{f \in \mathcal{F}} d_{\mathcal{G}_{nn}}(\boldsymbol{\pi}_l, \boldsymbol{\pi}^f) \\
&= d_{\mathcal{G}_{nn}}(\boldsymbol{\pi}_l, \boldsymbol{\pi}^{f_l^*}) - d_{\mathcal{G}_{nn}}(\boldsymbol{\pi}_l, \boldsymbol{\pi}^{\tilde{f}}) \\
&= d_{\mathcal{G}_{nn}}(\boldsymbol{\pi}_l, \boldsymbol{\pi}^{f_l^*}) - d_{\mathcal{G}_{nn}}(\boldsymbol{\pi}_l, \boldsymbol{\pi}_l^{f_l^*}) \\
&\quad + d_{\mathcal{G}_{nn}}(\boldsymbol{\pi}_l, \boldsymbol{\pi}_l^{f_l^*}) - d_{\mathcal{G}_{nn}}(\boldsymbol{\pi}_l, \boldsymbol{\pi}^{\tilde{f}}) \\
&\leq \underbrace{d_{\mathcal{G}_{nn}}(\boldsymbol{\pi}_l, \boldsymbol{\pi}^{f_l^*}) - d_{\mathcal{G}_{nn}}(\boldsymbol{\pi}_l, \boldsymbol{\pi}_l^{f_l^*})}_{(1)} \\
&\quad + \underbrace{d_{\mathcal{G}_{nn}}(\boldsymbol{\pi}_l, \boldsymbol{\pi}_l^{f_l^*}) - d_{\mathcal{G}_{nn}}(\boldsymbol{\pi}_l, \boldsymbol{\pi}^{\tilde{f}})}_{(2)},
\end{aligned} \tag{19}$$

where the last line holds because  $f_l^* \in \mathcal{F}_1$  and that  $\mathcal{F}_2 = \mathcal{F}_1$  due to Assumption 2.

We further examine Terms (1) and (2) separately. For Term (1), we have that

$$\begin{aligned}
& d_{\mathcal{G}_{nn}}(\boldsymbol{\pi}_l, \boldsymbol{\pi}^{f_l^*}) - d_{\mathcal{G}_{nn}}(\boldsymbol{\pi}_l, \boldsymbol{\pi}_l^{f_l^*}) \\
&= \sup_{g \in \mathcal{G}_{nn}} [\boldsymbol{\pi}_l g - \boldsymbol{\pi}^{f_l^*} g] - \sup_{g \in \mathcal{G}_{nn}} [\boldsymbol{\pi}_l g - \boldsymbol{\pi}_l^{f_l^*} g] \\
&\leq \sup_{g \in \mathcal{G}_{nn}} [\boldsymbol{\pi}_l^{f_l^*} g - \boldsymbol{\pi}^{f_l^*} g].
\end{aligned} \tag{20}$$

By the same token, for Term (2) we get

$$d_{\mathcal{G}_{nn}}(\boldsymbol{\pi}_l, \boldsymbol{\pi}_l^{f_l^*}) - d_{\mathcal{G}_{nn}}(\boldsymbol{\pi}_l, \boldsymbol{\pi}^{\tilde{f}}) \leq \sup_{g \in \mathcal{G}_{nn}} [\boldsymbol{\pi}_l^{f_l^*} g - \boldsymbol{\pi}^{\tilde{f}} g]. \tag{21}$$

Both the RHS of (20) and (21) can be upper-bounded by

$$\begin{aligned}
& \sup_{g \in \mathcal{G}_{nn}} [\boldsymbol{\pi}_l^{f_l^*} g - \boldsymbol{\pi}^{\tilde{f}} g] \leq \sup_{f \in \mathcal{F}, g \in \mathcal{G}_{nn}} [\boldsymbol{\pi}_l^f g - \boldsymbol{\pi}^{\tilde{f}} g] \\
&= \sup_{h \in \mathcal{H}} [\boldsymbol{\pi}_l(\mathbf{x})h - \boldsymbol{\pi}(\mathbf{x})h],
\end{aligned}$$

for any  $\tilde{f}$ , with a slight abuse of notation to represent the marginal measure of  $\mathbf{x}$  as  $\boldsymbol{\pi}(\mathbf{x})$ . Recall that  $h(\mathbf{x}) = g(\mathbf{x}, f(\mathbf{x}))$ , so the above equality holds. We can then use Lemma 5 to get

$$\textcircled{2} \leq 4\hat{\mathfrak{R}}_n(\mathcal{H}) + \frac{3B_g B_{xz} \sqrt{2 \ln \delta^{-1}}}{\sqrt{n}},$$

with probability at least  $1 - \delta$ , where the above bound is agnostic to the true measure  $\pi$ .

To proceed, we need to prove the following lemma.

**Lemma 6.** *Recall the sets  $\mathcal{F}_2$ ,  $\mathcal{F}_3$ , and  $\mathcal{F}_4$  defined in Assumptions 2 and 3. Then, if  $f_u^* \in \mathcal{F}_2 \cap \mathcal{F}_3$ , we have  $f_u^* \in \mathcal{F}_4$ .*

**Proof of Lemma 6:** Suppose that there exists  $f' \in \mathcal{F}_2 \cap \mathcal{F}_3$  that is not in  $\mathcal{F}_2 \cap \mathcal{F}_4$ . This means there exists  $f^* \in \mathcal{F}_2 \cap \mathcal{F}_4$  such that the following identity holds

$$d_{\mathcal{G}_{nn}}(\pi_l, \pi_{ul}^{f^*}) < d_{\mathcal{G}_{nn}}(\pi_l, \pi_{ul}^{f'}). \quad (22)$$

Now, since both  $f' \in \mathcal{F}_2$  and  $f^* \in \mathcal{F}_2$ , we have  $\pi_l^{f^*} = \pi_l^{f'} = \pi_l$ . Therefore, for any  $f \in \mathcal{F}_2$ ,

$$\begin{aligned} d_{\mathcal{G}_{nn}}(\pi_l, \pi_{ul}^f) &= \sup_{g \in \mathcal{G}_{nn}} \left[ \pi_l g - \frac{n}{m+n} \pi_l^f g - \frac{m}{m+n} \pi_{ul}^f g \right] \\ &= \sup_{g \in \mathcal{G}_{nn}} \left[ \pi_l g - \frac{n}{m+n} \pi_l g - \frac{m}{m+n} \pi_{ul}^f g \right] \\ &= \frac{m}{m+n} \sup_{g \in \mathcal{G}_{nn}} (\pi_l g - \pi_{ul}^f g) \\ &= \frac{m}{m+n} d_{\mathcal{G}_{nn}}(\pi_l, \pi_{ul}^f). \end{aligned}$$

Applying above to  $f^*$  and  $f'$  and using the strict inequality (22) implies

$$d_{\mathcal{G}_{nn}}(\pi_l, \pi_{ul}^{f^*}) < d_{\mathcal{G}_{nn}}(\pi_l, \pi_{ul}^{f'}).$$

This contradicts  $f' \in \mathcal{F}_3 = \arg \inf_{f \in \mathcal{F}} d_{\mathcal{G}_{nn}}(\pi_l, \pi_{ul}^f)$ . Hence, the assumption  $f' \notin \mathcal{F}_2 \cap \mathcal{F}_4$  is false, and therefore  $f' \in \mathcal{F}_4$ .  $\square$

Now, notice that in (19), the RHS is bounded with the empirical measure  $\pi_l$  of fully observed data. However, for  $f_u^*$  where the estimator is learned with both fully observed and partially observed data, we have a stronger condition that provides a tighter bound. Since  $f_u^*$  is learned with MCR,  $f_u^* \in \mathcal{F}_2 \cap \mathcal{F}_3$ . Therefore, by Lemma 6,  $f_u^* \in \mathcal{F}_4$ . Then, we obtain that

$$\begin{aligned} d_{\mathcal{G}_{nn}}(\pi_l, \pi_{ul}^{f_u^*}) &- \inf_{f \in \mathcal{F}} d_{\mathcal{G}_{nn}}(\pi_l, \pi^f) \\ &\leq d_{\mathcal{G}_{nn}}(\pi_l, \pi_{ul}^{f_u^*}) - d_{\mathcal{G}_{nn}}(\pi_l, \pi_{ul}^{f_u^*}) \\ &\quad + d_{\mathcal{G}_{nn}}(\pi_l, \pi_{ul}^{f_u^*}) - d_{\mathcal{G}_{nn}}(\pi_l, \pi^f). \end{aligned}$$

Following the same idea as derivations in (20) and (21), we have that for a prediction function  $f_u^*$  learned with MCR, Term ② is bounded above with probability at least  $1 - \delta$ , such that

$$\textcircled{2} \leq 4\hat{\mathfrak{R}}_{m+n}(\mathcal{H}) + \frac{3B_g B_{xz} \sqrt{2 \ln \delta^{-1}}}{\sqrt{m+n}}.$$

Adding the bounds derived for Term ② in each case (with and without MCR) to the bound (18) for general Terms ① and ③ completes the proof.  $\square$

*Dominance Relationship Derivation:* For simplicity, we drop the subscript for empirical distribution in this proof and let  $\pi$  denote the empirical distribution on the dataset  $\mathbf{D} = \{(\mathbf{x}_i, \mathbf{z}_i)\}_{i=1}^n$ , i.e.  $\pi := \frac{1}{n} \sum_{i=1}^n \delta_{(\mathbf{x}_i, \mathbf{z}_i)}$ . Given a predictor  $f : \mathcal{X} \rightarrow \mathcal{Z}$ , define the empirical *imputed* measure

$$\pi^f := \frac{1}{n} \sum_{i=1}^n \delta_{(\mathbf{x}_i, f(\mathbf{x}_i))}.$$

Define a coupling  $\psi$  between  $\pi$  and  $\pi^f$  by pairing the  $i$ -th atoms:

$$\psi := \frac{1}{n} \sum_{i=1}^n \delta_{((\mathbf{x}_i, \mathbf{z}_i), (\mathbf{x}_i, f(\mathbf{x}_i)))}.$$

Then  $\psi$  has marginals  $\pi$  and  $\pi^f$ .

**Case 1:**  $\mathcal{G}_{nn} = \{g : g \text{ is 1-Lipschitz}\}$  and  $\mathcal{L}_1(\mathbf{z}, \hat{\mathbf{z}}) = \|\mathbf{z} - \hat{\mathbf{z}}\|_1$ .

Assume the underlying metric on the joint space is

$$d((\mathbf{x}, \mathbf{z}), (\mathbf{x}', \mathbf{z}')) := \|\mathbf{z} - \mathbf{z}'\|_2.$$

For any  $g \in \mathcal{G}_{nn}$  and each sample index  $i$ , by 1-Lipschitz continuity,

$$\begin{aligned} &g(\mathbf{x}_i, \mathbf{z}_i) - g(\mathbf{x}_i, f(\mathbf{x}_i)) \\ &\leq |g(\mathbf{x}_i, \mathbf{z}_i) - g(\mathbf{x}_i, f(\mathbf{x}_i))| \\ &\leq d((\mathbf{x}_i, \mathbf{z}_i), (\mathbf{x}_i, f(\mathbf{x}_i))) = \|\mathbf{z}_i - f(\mathbf{x}_i)\|_2. \end{aligned}$$

Using the standard norm inequality  $\|\mathbf{v}\|_2 \leq \|\mathbf{v}\|_1$  for all  $\mathbf{v} \in \mathbb{R}^d$ ,

$$g(\mathbf{x}_i, \mathbf{z}_i) - g(\mathbf{x}_i, f(\mathbf{x}_i)) \leq \|\mathbf{z}_i - f(\mathbf{x}_i)\|_1.$$

Averaging and taking the supremum over  $g$  yields

$$\begin{aligned} d_{\mathcal{G}_{nn}}(\pi, \pi^f) &= \sup_{\text{Lip}(g) \leq 1} \frac{1}{n} \sum_{i=1}^n (g(\mathbf{x}_i, \mathbf{z}_i) - g(\mathbf{x}_i, f(\mathbf{x}_i))) \\ &\leq \frac{1}{n} \sum_{i=1}^n \|\mathbf{z}_i - f(\mathbf{x}_i)\|_1 = \pi \mathcal{L}_1. \end{aligned}$$

Therefore, the neural distance is  $(C, \alpha)$ -dominated by vector MAE with

$$(C, \alpha) = (1, 1).$$

**Case 2:**  $\mathcal{G}_{nn} = \{g : g \text{ is 1-Lipschitz}\}$  and squared loss.

With the same metric  $d((\mathbf{x}, \mathbf{z}), (\mathbf{x}', \mathbf{z}')) = \|\mathbf{z} - \mathbf{z}'\|_2$ , the previous argument gives  $d_{\mathcal{G}_{nn}}(\pi, \pi^f) \leq \pi \|\mathbf{z} - \hat{\mathbf{z}}\|_2$ . Then by Cauchy–Schwarz inequality,

$$\pi \|\mathbf{z} - \hat{\mathbf{z}}\|_2 \leq \sqrt{\pi \|\mathbf{z} - \hat{\mathbf{z}}\|_2^2}.$$

Therefore, if we define  $\mathcal{L}_2(\mathbf{z}, \hat{\mathbf{z}}) := \|\mathbf{z} - \hat{\mathbf{z}}\|_2^2$ , we have

$$d_{\mathcal{G}_{nn}}(\pi, \pi^f) \leq (\pi \mathcal{L}_2)^{1/2}.$$

So  $(C, \alpha) = (1, 1/2)$  for the squared loss.

**Case 3:**  $\mathcal{G}_{nn} = \{g : \|g\|_\infty \leq 1\}$  and excess NLL.

Let  $\pi$  now denote a (possibly population) joint distribution on  $(\mathbf{x}, \mathbf{z})$ , with conditional density  $p(\mathbf{z}|\mathbf{x})$ , and let  $\pi^f$  be a model distribution with conditional density  $q_f(\mathbf{z}|\mathbf{x})$  but the same  $\pi(\mathbf{x})$ , the marginal distribution on  $\mathbf{x}$  component. For  $\mathcal{G}_\infty := \{g : \|g\|_\infty \leq 1\}$ ,

$$d_{\mathcal{G}_\infty}(\pi, \pi^f) = \sup_{\|g\|_\infty \leq 1} [\mathbb{E}_\pi[g] - \mathbb{E}_{\pi^f}[g]] = 2 \text{TV}(\pi, \pi^f),$$

where  $\text{TV}$  denotes total variation distance. By Pinsker's inequality,

$$\text{TV}(\pi, \pi^f) \leq \sqrt{\frac{1}{2} \text{KL}(\pi \|\pi^f)}.$$

TABLE IV  
RATIO TEST HYPERPARAMETER

$\alpha_1$	$\alpha_2$	$\alpha_3$	$\beta_1$	$\beta_2$	$\lambda_w$	$\lambda_\nabla$	$\lambda_d$	$n_f$	$n_g$
0.002	0.0015	0.0015	0.9	0.999	0.01	10	0.01	4000	1

Combining the two inequalities yields

$$d_{\mathcal{G}_\infty}(\boldsymbol{\pi}, \boldsymbol{\pi}^f) \leq 2\sqrt{\frac{1}{2} \text{KL}(\boldsymbol{\pi} \|\boldsymbol{\pi}^f)} = \sqrt{2 \text{KL}(\boldsymbol{\pi} \|\boldsymbol{\pi}^f)}.$$

Finally, under the shared-marginal condition on  $\mathbf{x}$ ,

$$\begin{aligned} \text{KL}(\boldsymbol{\pi} \|\boldsymbol{\pi}^f) &= \mathbb{E}_{\boldsymbol{\pi}(\mathbf{x})} \left[ \text{KL}(p(\mathbf{z}|\mathbf{x}) \|\ q_f(\mathbf{z}|\mathbf{x})) \right] \\ &= \mathbb{E}_{\boldsymbol{\pi}} \left[ -\log q_f(\mathbf{z}|\mathbf{x}) + \log p(\mathbf{z}|\mathbf{x}) \right] \\ &=: \boldsymbol{\pi} \mathcal{L}_{NLL}. \end{aligned}$$

Hence

$$d_{\mathcal{G}_\infty}(\boldsymbol{\pi}, \boldsymbol{\pi}^f) \leq \sqrt{2 \boldsymbol{\pi} \mathcal{L}_{NLL}} = \sqrt{2} (\boldsymbol{\pi} \mathcal{L}_{NLL})^{1/2}.$$

So  $(C, \alpha) = (\sqrt{2}, 1/2)$ .

**Case 4:**  $\mathcal{G}_{nn} = \{g \in \mathcal{V} : \|g\|_{\mathcal{V}} \leq 1\}$  and  $\mathcal{L}_{\mathcal{V}}(\mathbf{z}, \hat{\mathbf{z}}) = \|\phi(\mathbf{z}) - \phi(\hat{\mathbf{z}})\|_{\mathcal{V}}^2$ .

Let  $\mathcal{V}$  be an RKHS with feature map  $\phi$ . For  $\mathcal{G}_{\mathcal{V}} := \{g \in \mathcal{V} : \|g\|_{\mathcal{V}} \leq 1\}$ , the IPM equals the MMD:

$$d_{\mathcal{G}_{\mathcal{V}}}(\boldsymbol{\pi}, \boldsymbol{\pi}^f) = \left\| \mathbb{E}_{\boldsymbol{\pi}}[\phi(\mathbf{z})] - \mathbb{E}_{\boldsymbol{\pi}^f}[\phi(\mathbf{z})] \right\|_{\mathcal{V}}.$$

Under the coupling  $\psi$  that pairs  $(\mathbf{x}_i, \mathbf{z}_i)$  with  $(\mathbf{x}_i, f(\mathbf{x}_i))$ , we can write

$$\mathbb{E}_{\boldsymbol{\pi}}[\phi(\mathbf{z})] - \mathbb{E}_{\boldsymbol{\pi}^f}[\phi(\mathbf{z})] = \mathbb{E}_{\psi}[\phi(\mathbf{z}) - \phi(\hat{\mathbf{z}})].$$

Then Jensen's inequality gives

$$\begin{aligned} d_{\mathcal{G}_{\mathcal{V}}}(\boldsymbol{\pi}, \boldsymbol{\pi}^f) &= \left\| \mathbb{E}_{\psi}[\phi(\mathbf{z}) - \phi(\hat{\mathbf{z}})] \right\|_{\mathcal{V}} \\ &\leq \mathbb{E}_{\psi} \left[ \|\phi(\mathbf{z}) - \phi(\hat{\mathbf{z}})\|_{\mathcal{V}} \right] \\ &\leq \sqrt{\mathbb{E}_{\psi} \left[ \|\phi(\mathbf{z}) - \phi(\hat{\mathbf{z}})\|_{\mathcal{V}}^2 \right]}. \end{aligned}$$

For the empirical coupling, this last quantity is exactly  $\sqrt{\boldsymbol{\pi} \mathcal{L}_{\mathcal{V}}}$ . Therefore

$$d_{\mathcal{G}_{\mathcal{V}}}(\boldsymbol{\pi}, \boldsymbol{\pi}^f) \leq (\boldsymbol{\pi} \mathcal{L}_{\mathcal{V}})^{1/2},$$

so  $(C, \alpha) = (1, 1/2)$ .

*Proof of Theorem 2:* Some of the proof for Theorem 2 follows the proof of Theorem 1. In fact, notice that the error decomposition in Eq. (15) breaks down the generalization error into Terms ①, ②, and ③, where Terms ① and ③ can be upper bounded independently for any learned prediction function. Therefore, the same upper bound holds, and we only need to focus on Term ② in this section. Recall that in Lemma 6, we defined  $f_l^* \in \mathcal{F}_2$  and proved  $f_u^* \in \mathcal{F}_4$ . Now, consider a function  $f'$  as a result of imperfect training, where  $\boldsymbol{\pi}_l \mathcal{L}^{f'} = \epsilon_{\mathcal{L}}$

and revisit the decomposition of Eq. (19). More specifically, for the case of learning without MCR, we have

$$\begin{aligned} d_{\mathcal{G}_{nn}}(\boldsymbol{\pi}_l, \boldsymbol{\pi}^{f'}) &- \inf_{f \in \mathcal{F}} d_{\mathcal{G}_{nn}}(\boldsymbol{\pi}_l, \boldsymbol{\pi}^f) \\ &= d_{\mathcal{G}_{nn}}(\boldsymbol{\pi}_l, \boldsymbol{\pi}^{f'}) - d_{\mathcal{G}_{nn}}(\boldsymbol{\pi}_l, \boldsymbol{\pi}^{\tilde{f}}) \\ &= d_{\mathcal{G}_{nn}}(\boldsymbol{\pi}_l, \boldsymbol{\pi}^{f'}) - d_{\mathcal{G}_{nn}}(\boldsymbol{\pi}_l, \boldsymbol{\pi}_l^{f'}) \\ &\quad + d_{\mathcal{G}_{nn}}(\boldsymbol{\pi}_l, \boldsymbol{\pi}_l^{f'}) - d_{\mathcal{G}_{nn}}(\boldsymbol{\pi}_l, \boldsymbol{\pi}_l^{f^*}) \\ &\quad + d_{\mathcal{G}_{nn}}(\boldsymbol{\pi}_l, \boldsymbol{\pi}_l^{f^*}) - d_{\mathcal{G}_{nn}}(\boldsymbol{\pi}_l, \boldsymbol{\pi}^{\tilde{f}}) \\ &\leq \underbrace{d_{\mathcal{G}_{nn}}(\boldsymbol{\pi}_l, \boldsymbol{\pi}^{f'}) - d_{\mathcal{G}_{nn}}(\boldsymbol{\pi}_l, \boldsymbol{\pi}_l^{f'})}_{(1)} \\ &\quad + \underbrace{d_{\mathcal{G}_{nn}}(\boldsymbol{\pi}_l, \boldsymbol{\pi}_l^{f'}) - d_{\mathcal{G}_{nn}}(\boldsymbol{\pi}_l, \boldsymbol{\pi}_l^{f^*})}_{(2)} \\ &\quad + \underbrace{d_{\mathcal{G}_{nn}}(\boldsymbol{\pi}_l, \boldsymbol{\pi}_l^{f^*}) - d_{\mathcal{G}_{nn}}(\boldsymbol{\pi}_l, \boldsymbol{\pi}^{\tilde{f}})}_{(3)}. \end{aligned} \tag{23}$$

Observe that in Eq. (23), we can upper bound Terms (1) and (3) in the same fashion as we did in the proof of Theorem 1 and reach the identical bound. Therefore, the only extra term to consider is Term (2). By interpolation, we also have  $d_{\mathcal{G}_{nn}}(\boldsymbol{\pi}_l, \boldsymbol{\pi}_l^{f^*}) = 0$ . So, Term (2) can simply be upper bounded by the dominance assumption (Assumption 4) as

$$d_{\mathcal{G}_{nn}}(\boldsymbol{\pi}_l, \boldsymbol{\pi}_l^{f'}) \leq C(\epsilon_{\mathcal{L}})^\alpha.$$

Adding it to the original bound, we have the estimation error for learning without MCR under imperfect training.

In the case of imperfect training with MCR, we also follow the proof for Theorem 1 with the following decomposition

$$\begin{aligned} d_{\mathcal{G}_{nn}}(\boldsymbol{\pi}_l, \boldsymbol{\pi}^{f'}) &- \inf_{f \in \mathcal{F}} d_{\mathcal{G}_{nn}}(\boldsymbol{\pi}_l, \boldsymbol{\pi}^f) \\ &\leq \underbrace{d_{\mathcal{G}_{nn}}(\boldsymbol{\pi}_l, \boldsymbol{\pi}^{f'}) - d_{\mathcal{G}_{nn}}(\boldsymbol{\pi}_l, \boldsymbol{\pi}_{ul}^{f'})}_{(1)} \\ &\quad + \underbrace{d_{\mathcal{G}_{nn}}(\boldsymbol{\pi}_l, \boldsymbol{\pi}_{ul}^{f'}) - d_{\mathcal{G}_{nn}}(\boldsymbol{\pi}_l, \boldsymbol{\pi}_{ul}^{f^*})}_{(2)} \\ &\quad + \underbrace{d_{\mathcal{G}_{nn}}(\boldsymbol{\pi}_l, \boldsymbol{\pi}_{ul}^{f^*}) - d_{\mathcal{G}_{nn}}(\boldsymbol{\pi}_l, \boldsymbol{\pi}^{\tilde{f}})}_{(3)}. \end{aligned}$$

Again, we have bounded term (1) and (3) previously for the MCR case, therefore, the only addition to the estimation error would be term (2) here. We proceed with the following decomposition

TABLE V

CAPACITY TEST HYPERPARAMETERS, THE FIRST BLOCK ARE HYPERPARAMETERS FOR VARYING WIDTH TEST, AND THE SECOND BLOCK ARE HYPERPARAMETERS FOR VARYING DEPTH TEST. THE LEFT COLUMN SHOWS THE SPECIFIC TEST SETTING (VALUE FOR WIDTH OR DEPTH).

	$\alpha_1$	$\alpha_2$	$\alpha_3$	$\beta_1$	$\beta_2$	$\lambda_w$	$\lambda_\nabla$	$\lambda_d$	$n_f$	$n_g$
16	0.005	0.005	0.0015	0.9	0.999	0.01	10	0.01	4000	1
32	0.0025	0.0025	0.0015	0.9	0.999	0.01	10	0.01	4000	1
64	0.002	0.0015	0.0015	0.9	0.999	0.01	10	0.01	4000	1
128	0.0015	0.0015	0.0015	0.9	0.99	0.01	10	0.01	4000	1
256	0.0011	0.0011	0.0015	0.9	0.95	0.01	10	0.01	4000	1
2	0.005	0.005	0.0015	0.9	0.999	0.01	10	0.01	4000	1
4	0.001	0.001	0.0015	0.9	0.999	0.01	10	0.01	4000	1
6	0.0005	0.0005	0.0015	0.9	0.999	0.01	10	0.01	4000	1

TABLE VI  
DUALITY GAP STOPPING CONDITION EVALUATION HYPERPARAMETER

$\alpha_1$	$\alpha_2$	$\alpha_3$	$\beta_1$	$\beta_2$	$\lambda_w$	$\lambda_\nabla$	$\lambda_d$	$n_f$	$n_g$
0.005	0.005	0.005	0.9	0.999	0.01	10	0.01	2000	1

TABLE VII  
MCR WEIGHT  $\lambda_d$  EVALUATION HYPERPARAMETER

$\alpha_1$	$\alpha_2$	$\alpha_3$	$\beta_1$	$\beta_2$	$\lambda_w$	$\lambda_\nabla$	$n_f$	$n_g$
0.005	0.005	0.0015	0.9	0.99	0	10	2000	1

TABLE VIII  
NEURAL NET DISTANCE EVALUATION HYPERPARAMETER

$\alpha_1$	$\alpha_2$	$\alpha_3$	$\beta_1$	$\beta_2$	$\lambda_w$	$\lambda_\nabla$	$n_f$	$n_g$
0.005	0.002	0.0015	0.9	0.99	0	10	2000	1

$$\begin{aligned}
& d_{\mathcal{G}_{nn}}(\pi_l, \pi_{ul}^{f'}) - d_{\mathcal{G}_{nn}}(\pi_l, \pi_{ul}^{f_u^*}) \\
&= \sup_{g \in \mathcal{G}_{nn}} [\pi_l g - \pi_{ul}^{f'} g] - \sup_{g \in \mathcal{G}_{nn}} [\pi_l g - \pi_{ul}^{f_u^*} g] \\
&\leq \sup_{g \in \mathcal{G}_{nn}} [\pi_{ul}^{f'} g - \pi_{ul}^{f_u^*} g] \\
&= \sup_{g \in \mathcal{G}_{nn}} \left[ \frac{n}{m+n} (\pi_l^{f'} g - \pi_l^{f_u^*} g) + \frac{m}{m+n} (\pi_u^{f'} g - \pi_u^{f_u^*} g) \right] \\
&\leq \frac{n}{m+n} \sup_{g \in \mathcal{G}_{nn}} [\pi_l^{f'} g - \pi_l^{f_u^*} g] + \frac{m}{m+n} \sup_{g \in \mathcal{G}_{nn}} [\pi_u^{f'} g - \pi_u^{f_u^*} g] \\
&= \frac{n}{m+n} d_{\mathcal{G}_{nn}}(\pi_l^{f'}, \pi_l^{f_u^*}) + \frac{m}{m+n} d_{\mathcal{G}_{nn}}(\pi_u^{f'}, \pi_u^{f_u^*}) \\
&\leq \frac{n}{m+n} C(\epsilon_{\mathcal{L}})^\alpha + \frac{m}{m+n} (d_{\mathcal{G}_{nn}}(\pi_u^{f'}, \pi_l) + d_{\mathcal{G}_{nn}}(\pi_l, \pi_u^{f_u^*})) \\
&\leq \frac{n}{m+n} C(\epsilon_{\mathcal{L}})^\alpha + \frac{m}{m+n} (\epsilon_d + 2\xi),
\end{aligned}$$

where the last line follows from the definitions of  $\epsilon_d$  and  $\xi$ . Adding above to the original estimation error bound for MCR completes the proof.  $\square$

### Simulation Settings

Throughout this section, we will use consistent notation for all optimization hyperparameters. We use  $\alpha_1$  for the learning rate of the model trained without MCR.  $\alpha_2$  for learning rate of the model trained with MCR.  $\alpha_3$  for the learning rate of the neural distance function  $g$ .  $\beta_1$ ,  $\beta_2$ , and  $\lambda_w$  are the parameters of the AdamW algorithm.  $\lambda_\nabla$  is the weight for

the gradient penalty.  $\lambda_d$  is the weight of the neural distance penalty.  $n_f$  for the maximum epoch number for updating the prediction function  $f$ ,  $n_g$  for the epoch number for updating neural distance function  $g$ .

*Verifying Theoretical Claims:* For comparison of the  $m$  and  $n$  ratios, we set  $d_x = 30$ ,  $d_z = 20$ . The generation process is achieved with randomly initialized two-layer ReLU activation MLP with 64 neurons in the first hidden layer and 32 in the second hidden layer. The prediction function is also a two-hidden-layer MLP with ReLU activation and batch normalization; both hidden layers have 64 neurons. The neural distance function is another two-hidden-layer ReLU activation MLP with 512 neurons in the first hidden layer and 256 neurons in the second hidden layer.

In the learning process, the primary loss function  $\mathcal{L}$  is the mean squared error loss, and the optimizer is AdamW. The hyperparameter settings are shown in Table IV.

For model capacity comparison, we follow the same data generation process as described earlier. However, we always generate 100 fully observed training data, 1000 partially observed data for penalty calculation, and 2000 fully observed test data. For varying the model width, we set the depth of the MLP prediction function to 2 (two hidden layers). For varying the depth of the model, we set the width of the model to 64. We also use the same neural distance function. The hyperparameter settings are shown in Table V.

For MCR weight  $\lambda_d$  comparison, we set  $m = 2000$  and  $n = 100$ , and the parameter settings are shown in Table VII.

TABLE IX  
DISTRIBUTION DISCREPANCY EVALUATION HYPERPARAMETER

$\alpha_1$	$\alpha_2$	$\alpha_3$	$\beta_1$	$\beta_2$	$\lambda_w$	$\lambda_\nabla$	$\lambda_d$	$n_f$	$n_g$
0.005	0.005	0.0015	0.9	0.99	0	10	0.01	2000	1

TABLE X  
IMAGE RECONSTRUCTION HYPERPARAMETERS, FIRST ROW FOR MNIST, SECOND ROW FOR CIFAR 10.

$\alpha_1$	$\alpha_2$	$\alpha_3$	$\beta_1$	$\beta_2$	$\lambda_w$	$\lambda_\nabla$	$\lambda_d$	$n_f$	$n_g$
0.0001	0.00015	0.0001	0.9	0.999	0.01	10	0.01	500	2
0.00001	0.00001	0.001	0.9	0.99	0.01	10	0.02	500	3

TABLE XI  
SENSOR DATA IMPUTATION HYPERPARAMETERS, FIRST ROW FOR ACVITITY, SECOND ROW FOR CROP.

$\alpha_1$	$\alpha_2$	$\alpha_3$	$\beta_1$	$\beta_2$	$\lambda_w$	$\lambda_\nabla$	$\lambda_d$	$n_f$	$n_g$
0.0005	0.0005	0.001	0.9	0.999	0.01	10	0.01	5000	2
0.0003	0.0003	0.001	0.9	0.999	0.01	10	0.01	5000	2

TABLE XII  
SINGLE CELL DATA IMPUTATION HYPERPARAMETERS.

$\alpha_1$	$\alpha_2$	$\alpha_3$	$\beta_1$	$\beta_2$	$\lambda_w$	$\lambda_\nabla$	$\lambda_d$	$n_f$	$n_g$
0.0001	0.0001	0.0001	0.9	0.95	0.01	10	0.001	1000	5

For choice of neural net distance  $\mathcal{G}_{nn}$ , the hyperparameters settings are shown in Table VIII. Note that the only difference between MMD and 1-Wasserstein MCR hyperparameters settings is the  $\lambda_d$  values, in consideration of the loss scales to ensure the primary MSE loss converges to similar values in both scenarios.

For the distribution discrepancy  $\hat{\xi}$  evaluation, the hyperparameters settings are shown in Table IX.

*Evaluating Duality Gap Stopping Condition:* We use the same synthetic data generation process as in the previous section, with  $n$  set to 100 and  $m$  set to 2000. The hyperparameters settings are shown in Figure VI. For duality gap estimation, we set the duality gap update step to  $n_d = 5$  for a more accurate estimation.

#### Versatility of MCR:

#### Image Reconstruction

For the MNIST reconstruction experiment, we normalize the data to  $[0, 1]$  by dividing it by 255. For the CIFAR10 dataset, we do the same thing, while cropping out along the pixel dimension. For both datasets, we choose 1000 data points as fully observed training data, 5000 cropped images as penalty data, and the rest as test data. For the prediction function  $f$ , we choose a convolutional autoencoder with convolution filters in the encoder and convolution transpose in the decoder. The encoder and decoder have a mirror structure, with 32 channels in the first layer and 64 channels in the second layer. The latent dimension is 32 for MNIST and 128 for CIFAR. We use the ReLU activation function. The neural distance function now has convolution filters with 16 channels, followed by a linear layer. We also use the AdamW optimizer. The hyperparameter setting is shown in Table X, where the first row is for MNIST and the second row is for CIFAR10.

#### Sensor Data Imputation

For the Activity dataset, we standardize the data set to mean 0 and standard deviation 1 along each feature dimension. We sample 400 data points as fully observed training data, and 2000 TEB and EDA data for neural distance penalty. The rest of the dataset are used as test data. For the Crop dataset, we do the same standardization procedure, and we sample 1000 data as fully observed training data, and 5000 radar data for neural distance penalty. For the prediction function  $f$ , we use variational autoencoders. Again, encoder and decoder has mirror structures, with the first layer of width 512, and second layer of width 256 for both datasets, and a latent dimension of 128 for Activity dataset, and 32 for crop dataset. We use the same MLP neural distance function  $g$  as before. The optimization hyperparameter setting is shown in Table XI. First row is for Activity dataset, and the second row is for Crop dataset.

#### Single Cell Data Integration

Due to a lack of data points in the scMultiSim dataset, we only divide the datasets into two parts. The first part is 200 fully observed training data, and the second part contains 300 RNA count for neural distance penalty calculation and 300 ATAC-seq data for testing. We follow the same data normalization approach in [17]. For the prediction function  $f$ , we write a custom version of MultiVI [13] by removing the module that encodes library size, since we only have access to two data modalities. Moreover, we set the weighting factor for KL divergence in the latent space to 10. We use the same MLP neural net distance function  $g$  as before as it still works well in this case. The hyperparameter setting is shown in Table XII.